Research Square

Preprints are preliminary reports that have not undergone peer review.
They should not be considered conclusive, used to inform clinical practice,
or referenced by the media as validated information.

Preliminary geochemical analyses indicate the potential for chemostratigraphic correlations within the Crato Formation Konservat-Lagerstätte (Cretaceous), Araripe Basin, Brazil

Leonardo Corecco

leonardoqueiroz@unipampa.edu.br

Universidade Federal do Pampa, Caçapava do Sul (RS)

Igor Hamid

Federal University of Ceará

Vitor P. Pereira

Universidade Federal do Rio Grande do Sul – Porto Alegre (RS)

Lucas Bonan-Gomes

Universidade Federal do Rio Grande do Sul - Porto Alegre (RS)

Artur F.S. Araujo

Universidade Regional do Cariri

Luiz R.S. Nascimento

Federal University of Ceará

Antônio Á.F. Saraiva

Regional University of Cariri

Duc Huy Dang

Trent University

Luiz D. Lacerda

Federal University of Ceará

Naiara C. Oliveira

Universidade Regional do Cariri

Marina B. Soares

Museu Nacional, Universidade Federal do Rio de Janeiro

Alexander W.A. Kellner

Museu Nacional, Universidade Federal do Rio de Janeiro

Renan A.M. Bantim

Universidade Regional do Cariri

Research Article

Keywords: Araripe Basin, Cretaceous, Fossil trade, Geochemical investigation, Trace elements

Posted Date: November 25th, 2026

DOI: https://doi.org/10.21203/rs.3.rs-11732024/v1

License: This work is licensed under a Creative Commons Attribution 4.0 International License.
Read Full License

Additional Declarations: No competing interests reported.

Preliminary geochemical analyses indicate the potential for chemostratigraphic correlations within the Crato Formation Konservat-Lagerstätte (Cretaceous), Araripe Basin, Brazil

Leonardo Corecco[a,b*], Igor Hamid[c], Vitor P. Pereira[d], Lucas Bonan-Gomes[e], Artur F.S. Araujo[b], Luiz R.S. Nascimento[c], Antônio Á.F. Saraiva[f], Duc Huy Dang[g], Luiz D. Lacerda[c], Naiara C. Oliveira[b,h], Marina B. Soares[i], Alexander W.A. Kellner[i], Renan A.M. Bantim[b,f,j]

[a] Departamento de Geologia, Universidade Federal do Pampa, Caçapava do Sul (RS), Brazil.

[b] Laboratório de Paleontologia, Universidade Regional do Cariri, Crato, Ceará, Brazil.

[c] Laboratório de Biogeoquímica Costeira (LBC), Marine Sciences of Institute, Federal University of Ceará, Fortaleza, CE, Brazil.

[d] Departamento de Mineralogia e Petrologia, Instituto de Geociências, Universidade Federal do Rio Grande do Sul – Porto Alegre (RS), Brazil.

[e] Departamento de Materiais, Escola de Engenharia, Universidade Federal do Rio Grande do Sul - Porto Alegre (RS), Brazil.

[f] Department of Biological Sciences, Regional University of Cariri, Crato, CE, Brazil.

[g] Department of Chemistry, Trent University, 1600 W Bank Dr, Peterborough, ON K9L0G2, Canada.

[h] Departamento de Física, Centro de Ciências e Tecnologia, Universidade Regional do Cariri, Juazeiro do Norte-CE, Brazil.

[i] Laboratório de Sistemática e Tafonomia de Vertebrados Fósseis (LAPUG), Setor de Paleovertebrados, Departamento de Geologia e Paleontologia, Museu Nacional, Universidade Federal do Rio de Janeiro, Rio de Janeiro, Brazil.

[j] Museu de Paleontologia Plácido Cidade Nuvens da Universidade Regional do Cariri, URCA, Santana do Cariri, CE, Brazil

Corresponding author: Leonardo Corecco (leonardoqueiroz@unipampa.edu.br)

Address: Departamento de Geologia, Universidade Federal do Pampa, Avenida Pedro Anunciação, 111 - Vila Batista, Caçapava do Sul (RS), CEP: 96570-000, Brazil.

ABSTRACT

The Araripe Basin is widely known for its rich and diversified paleontological record. Among the most important deposits is the Crato Formation, considered a Fossil Konservat-Lagerstätte whose geochemical characterization, despite decades of study, remains debated. Fossil illegal commercialization has been a significant threat to this paleontological heritage. Besides improving reconstructions of this exceptional Cretaceous ecosystem, chemostratigraphic characterization has the potential to characterize the layers or locality where the fossil material comes from and may help to recover lost fossil-provenance information, and eventually become a tool to relocate illegally collected specimens into their original stratigraphic context. Here we present a preliminary geochemical analysis (major and trace elements) of 45 samples collected from five major quarries (nine from each) in the municipalities of Nova Olinda and Santana do Cariri, from where fossils have been commercialized for decades. Elemental concentrations and enrichment factor calculations (EF_{Fe} and EF_{Al}) indicate differences in geochemistry across the laminated limestones of the Crato Formation, both within individual "*talhados*" (vertically) and among the different sampled outcrops (laterally), from the same unit. Two preliminary chemostratigraphic markers can be proposed: low Cu contents for tracking the lowermost layers and, with slightly lower consistency, high Ba and Ti values for tracking the upper layers. Moreover, the NW–SE to WNW–ESE-oriented fault may potentially influence the geochemical signatures of the *talhados* and on the proposed chemostratigraphic markers. The signatures established here show the potential of this approach for serving as a tool to reconstruct provenance of fossil specimens.

KEYWORDS: Araripe Basin, Cretaceous, Fossil trade, Geochemical investigation, Trace elements

1. Introduction

Colonialism, a political, economic, and social system characterized by a process of domination through which a nation maintains or extends its control over territories or communities (Michaelis Dictionary, 2026), originated in the fifteenth century and left profound and lasting impacts on Latin American societies, particularly through the exploitation of territories and natural resources. These practices also extended to the production and circulation of scientific knowledge, including the removal of specimens and the establishment of scientific collections in colonial powers (Aldrich, 2009). Natural heritage, including fossils, rocks, minerals, and other geological resources (Donnelly and Pirrie, 2024), was frequently removed from colonized territories and incorporated into public and private scientific collections in Europe (Araújo et al., 2024b). These historical processes may also have contributed to the

uneven global distribution of paleontological research, as approximately 97% of paleontological publications over the past 30 years have involved researchers and institutions based in North America and Western Europe (Raja et al., 2021).

In this context, the Araripe Basin represents one of the most important fossil-bearing regions of the Early Cretaceous in the Gondwana supercontinent. The Cretaceous deposits of the Araripe Basin, including the Santana Group, are closely related to the South Atlantic opening. From the base to the top, the Santana Group comprises four different formations: Barbalha, Crato, Ipubi, and Romualdo (Assine et al., 2014; Custódio et al., 2017), although some have used a different nomenclature (Martill, 2007), what has been challenged (see Kellner et al., 2013 for a short discussion).

The Crato Formation (Upper Aptian, Lower Cretaceous age), the focus of this study, represents a stratigraphic sequence of supposedly lacustrine deposits with a predominance of carbonates, with freshwater constituting the superficial and marginal portions of the lakes, and covering an area of about 5.000 km^2 (Neuman et al., 2003; Heimhofer and Martill, 2007; Storari et al., 2021). This unit was deposited under a stratified water column, with relatively well oxygenated upper layers, and reportedly anoxic lower layers, with records of several mortality events (Heimhofer and Martill, 2007; Saraiva et al., 2007; Heimhofer et al., 2010; Storari et al., 2021; Hamid et al., 2024b).

The Crato Formation is particularly notable for its high taxonomic diversity and exceptional fossil preservation, including insects, crustaceans, fish, lizards, turtles, crocodiles, pterosaurs, birds, dinosaurs, feathers and plants (e.g., Kellner and Saraiva, 2019). These characteristics led to its recognition as a Fossil Konservat-Lagerstätte, providing an exceptional record of Early Cretaceous continental ecosystems (Wilby and Martill, 1992; Kellner et al., 1994; Kellner and Campos, 2007; Figueiredo et al., 2011; Pinheiro et al., 2012; Oliveira and

Kellner, 2017; Warren et al., 2017; Cheng et al., 2018; Campos et al., 2019; Bezerra et al., 2021; Storari et al., 2021; Batista et al., 2024; Santos et al., 2025).

Despite its exceptional paleontological significance, the Araripe Basin exemplifies persistent inequalities in the collection, research, and ownership of paleontological heritage. Cisneros et al. (2022) examined 71 publications on vertebrates and plant macrofossils and found that 57% did not include Brazilian co-authors, while 88% of the holotypes were housed in foreign collections and had not been repatriated. Similarly, Macário et al. (2025) highlighted an alarming situation concerning macroinvertebrates from the Santana Group. According to these authors, about five hundred macroinvertebrate species have been described for the Santana Group. However, nearly half of the holotypes are housed in institutions outside Brazil. An additional concern is that more than two hundred species were described in publications that did not include any Brazilian scientists as co-authors (Macário et al., 2025).

The Decree Law Nº 4.146/42 of Brazil declares fossils as national assets, and that its extraction depends on prior authorization, as well as its supervision is the responsibility of the National Mining Agency (Agência Nacional de Mineração, ANM; Brasil, 1942). The illegal extraction and trade of paleontological specimens extend beyond the Araripe Basin, reflecting persistent colonial and socioeconomic inequalities affecting fossil circulation and research in countries such as Dominican Republic, Brazil, Myanmar and Morocco (Raja et al., 2021; Cisneros et al., 2022). Despite that, there is no agreement about the Brazilian fossil's cultural heritage (Araújo-Júnior, 2023; Kellner, 2023b; Araújo-Júnior et al., 2024a, b; Kuhn et al., 2023, 2024).

Nevertheless, due to social vulnerability existing in this region, it is not uncommon to see illegal trade or even trafficking of materials originating from the Araripe Basin (Cisneros et al., 2022; Kellner, 2023a, b).

Efforts by Brazilian researchers and scientific and governmental institutions have strengthened heritage protection (Araújo-Júnior et al., 2024a). Notwithstanding, although the repatriation of *Ubirajara jubatus*, for example, represents an important milestone (Lenharo and Rodrigues, 2022; Stewens, 2023), the case of *Irritator challenger*, another type specimen from Araripe Basin, demonstrates that the repatriation of Brazilian fossils remains unresolved.

Beyond repatriation, the removal of fossils from their geological context creates a major challenge of determining the provenance of specimens which the incomplete or unavailable information on fieldwork, collection history, and export permits (Araújo-Júnior, 2023; Gelsthorpe, 2024; Araújo-Júnior et al. 2024a; Macário et al. 2025). Hampering establishing their geographic and stratigraphic provenance, essential for legal and cultural attribution and for interpreting their paleoenvironmental, biogeographic, and evolutionary significance (Sacchi and Nicosia 2013; Donnelly and Pirrie 2024).

Notwithstanding its paleontological significance, few studies have focused on the geochemical characterization of the layers that compose the Crato Formation (e.g., Heimhofer et al., 2010; Corecco et al., 2022; Hamid et al., 2024b). Within this context, this study aims to preliminary characterize the geochemistry of the laminated limestone of the Crato Formation (C5 facies) from five quarries (outcrops) in the municipalities of Nova Olinda and Santana do Cariri (Ceará, Brazil) to assess chemostratigraphic correlations at stratigraphic layer level. This approach can assist discussions on the provenance of illegally collected fossils that were illegally taken out of the country, by enabling their stratigraphic and outcrop-level positioning.

2. Geological setting and geochemical background

The intracratonic Araripe Basin is located in the northeastern region of Brazil, outcropping among the states of Ceará, Pernambuco and Piauí, with an area of about 9,000 km^2 (Ponte and Ponte Filho, 1996; Fig. 1). This sedimentary basin preserves a comprehensive

record of the opening of the Atlantic Ocean, associated with the fragmentation of the Gondwana supercontinent (Assine, 2007). Its depositional succession spans the Ordovician (Cerri et al., 2024), and Late Jurassic to Early Cretaceous and is subdivided into five tectonodepositional systems: syneclise, pre-rift, rift, and post-rift I and II (Assine, 2007; Fambrini et al., 2020). Within this tectonosedimentary framework, the Crato Formation constitutes part of the Santana Group, which comprises, from base to top, the Barbalha, Crato, Ipubi and Romualdo formations (Assine et al., 2014).

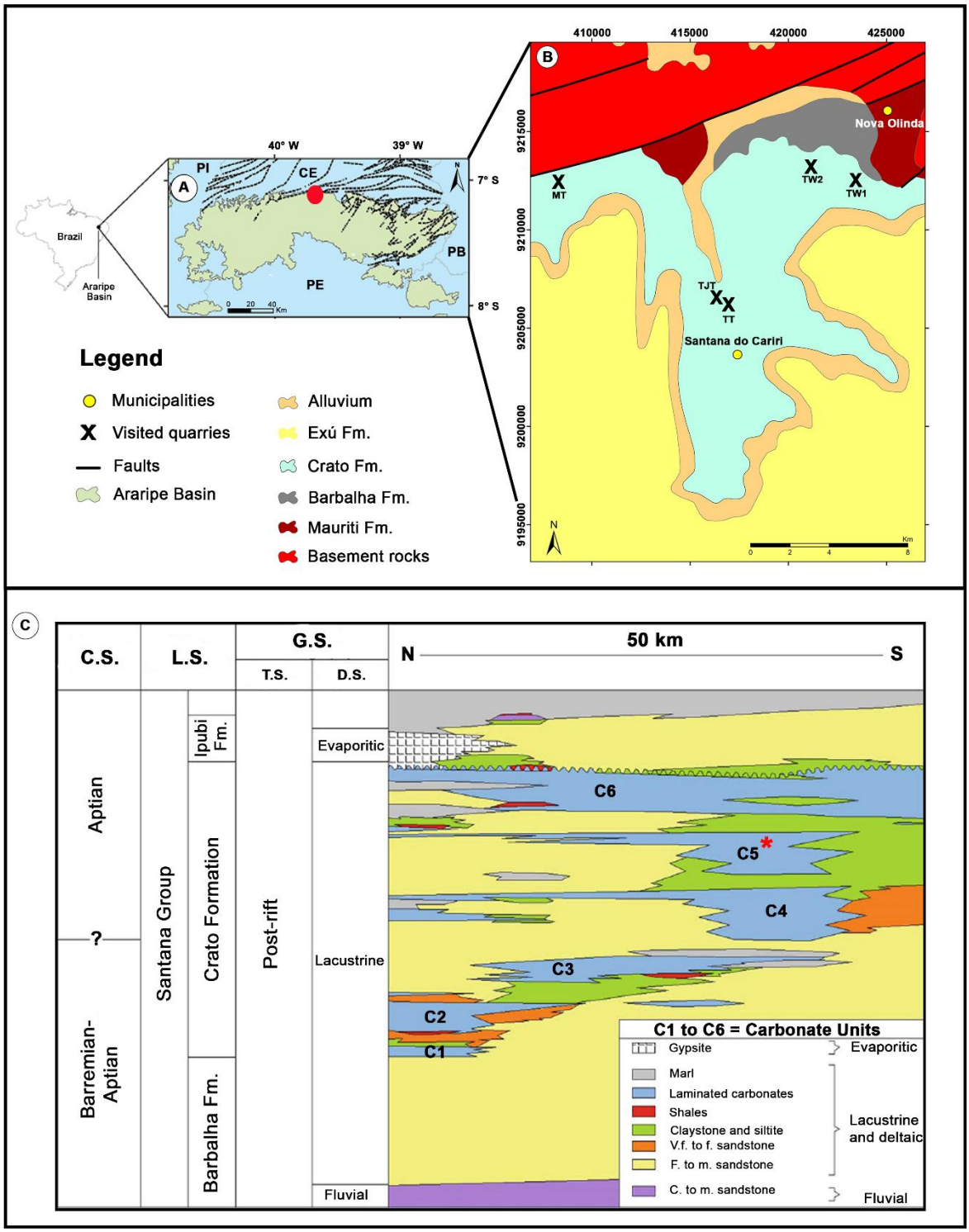

Figure 1

The Crato Formation can be divided into six informal units, from bottom to top, C1–C6, interlayered by sandstones, siltstones, and shales (Neumann and Cabrera, 1999). These six

carbonate facies can be found on the municipalities of Santana do Cariri and Nova Olinda, both in Ceará state, in a series of laminated limestone outcrops, usually located in commercial quarries or river margins on the Araripe Plateau, popularly named "*Talhados*" (Viana and Neumann, 2002; Corecco et al., 2022). These units were characterized based on their lithological–sedimentological contents and their type and amount of organic matter by Neumann et al. (2003) as follows: C1 - marginal lacustrine deltaic massive to coarsely laminated mudstones and sandstones found as lenticular sheet and channel-infills; C2 - oxic marginal lacustrine massive to poorly laminated mudstones; C3 - oxic–suboxic inner lacustrine mudstones and laminated bioclastic mudstones; C4 - anoxic, inner lacustrine dark mudstones; C5 - anoxic, inner lacustrine dark clay-carbonate rhythmites; and C6 - anoxic, inner lacustrine finely laminated dark micritic limestones (Fig. 1C). These facies make up decimeter- to several meter-thick parasequences, which stack up in several tens of meters thick successions. This study will deal with the C5 unit.

Despite representing a unique episode in the geological history of South America, chemostratigraphic studies in the Araripe Basin remain relatively scarce compared with the fossiliferous, sedimentological and stratigraphic research. Nevertheless, several studies stand out for their use of trace elements and stable isotopes. Heimhofer et al. (2010) applied high-resolution multiproxy techniques, such as detailed logging, petrography, μ-XRF scanning, and stable-isotope geochemistry, to reconstruct paleoenvironmental conditions from sample slabs from three local stratigraphic sections in the Araripe Basin and suggested a transition from closed or semi-closed conditions to a more open lake system during the onset of laminite deposition in the Crato Formation. Benigno et al. (2021) identified positive Hg excursions independent of organic carbon (C_{org}) accumulation during the depositional history of the Santana Group. They associated these excursions with contemporaneous volcanic events and suggested that local paleoenvironmental conditions may also have been influenced by these

events. Bom et al. (2021), Lúcio et al. (2022), and Salgado-Campos et al. (2021) documented modifications in paleosalinity, paleoproductivity, and paleoredox conditions in the Romualdo, Ipubi, and Crato formations, respectively. Castro et al. (2017), Pontes et al. (2021), and Varejão et al. (2021a, b) conducted isotopic investigations ($\delta^{13}C$, $\delta^{18}O$, and $\delta^{34}S$) to investigate oscillations in paleoproductivity and paleotemperature. Pontes et al. (2021) suggested extremely reducing conditions driven by bacterial sulfate reduction. Altogether, these studies mainly focus on the Aptian–Albian interval (~121.4–113 Ma) of the Lower Cretaceous. Recently, Pimentel de Sousa et al. (2025) suggested a preliminary distinctive isotopic signature ($\delta^{18}O$ and $\delta^{13}C$) for the Crato Formation fossil-bearing "Sete Cortes" ethnostratum. In parallel, Corecco et al. (2022) evaluated the feasibility of applying an informal lithostratigraphic approach (ethnostratigraphy) to describe the petrological and paleontological features of beds within the Crato Formation succession, testing whether quarry-worker stratigraphic subdivisions (e.g., “Matracão”, “Lajão dos Sete Cortes”) could support paleoenvironmental interpretations. More recently, Hamid et al. (2024a) characterized the paleoenvironmental geochemistry across the Aptian–Albian transition in the Araripe Basin, reconstructing depositional conditions for the Santana Group (Barbalha, Crato, and Romualdo formations) and establishing correlations with Oceanic Anoxic Events OAE-1a and OAE-1b. Hamid et al. (2024b) further assessed biostratigraphic correlations between mortality events recorded in the Crato Konservat-Lagerstätte and Lower Cretaceous chemostratigraphy, aiming to clarify the factors responsible for the cyclic mortality patterns documented in the Crato Formation, in the C6 unit of Neumann and Cabrera (1999) and Neumann et al. (2003). Finally, Antonietto et al. (2025) investigated the development of the paleotrophic chain in the Romualdo Formation Konservat-Lagerstätte using mercury (Hg) concentrations, revealing insights into the evolution of the paleoichthyofauna and the behavior of other organisms, such as pterosaurs. No previous study, however, has attempted to geochemically individualize multiple outcrops of the Crato

Formation (especially in C5 facies, *sensu* Neumann and Cabrera, 1999) aiming for chemostratigraphic markers that enable geographic correlations and fossil tracking.

The present study focused on five "*Talhados*" (quarries) of laminated limestone located in the municipalities of Santana do Cariri and Nova Olinda (Fig. 1 and 2). Macroscopically, the collected samples correspond to laminated and rhythmic calcilutites, containing microspathic to spathic calcite crystals. In addition to calcite, dolomite, ankerite, gipsite, goethite, hematite and anatase have previously been identified in this unit through X-ray Diffractometry (XRD) and petrographic analyses (Corecco et al., 2022).

3. Material and methods

Forty-five laminated limestone samples from five "*Talhados*" (nine from each) were collected. Twenty-five samples (five per quarry) were analyzed by flame atomic absorption spectrometry (FAAS), whereas the other twenty (four per quarry) were analyzed by Inductively Coupled Plasma Mass Spectrometry (ICP-MS, Agilent-8900®). These quarries encompass the Crato Formation layers (C5 unit; *sensu* Neumann and Cabrera, 1999; Fig. 1C and 2). Detailed information on location, altitude and major characteristics is listed in Supplementary Material S1.

3.1. Geochemical analyses

3.1.1. Flame atomic absorption spectrometry (FAAS) analyses

The concentrations of some major and trace elements (Al, Ti, V, Mn, Fe, Ni, Cu, Zn, Sr, Ba and Pb), in twenty-five samples, were determined by flame atomic absorption spectrometry (FAAS-7000, SHIMADZU®), at the Institute of Marine Sciences (LABOMAR) of the Federal University of Ceará (Fortaleza, Brazil). These elements were selected due to

222 their widespread occurrence in sedimentary carbonates (Turekian and Wedepohl, 1961) and
223 their potential to distinguish individual outcrops.

224 Each sample was powdered and analyzed in duplicate. Approximately 1.5 g of sample
225 were digested using 15 mL of 100% *aqua regia* solution (HCl: HNO_3, 3/1, v/v) in closed Teflon
226 tubes, with 30 minutes of pre-digestion in pressure vessels. The samples were then subjected
227 to a microwave (1600 W and 175°C for 20 minutes). The extracts were taken to 30 mL with
228 HNO_3 0.2 % v/v in volumetric flasks. All glassware was rigorously cleaned by a 24-hour
229 immersion in a 10% v/v Extran detergent solution (Fisher Scientific®), followed by a 24-hour
230 soaking in a 10% v/v HCl (Sigma-Aldrich®) solution. Standard reference materials (NIST-
231 1646A®), reagent blanks, and duplicate samples were meticulously prepared and analyzed to
232 assess the precision (70–97%). The calibration curves of each metal were prepared with
233 MERCK® standard solutions (1,000 μg mL^{-1}), and the procedure quantification limit was 0.03
234 to 0.69 μg g^{-1}. More information about recovery, detection limit (DL), and quantifications (LQ)
235 of each metal can be found in Supplementary Material S2.

236 *3.1.2. Inductively Coupled Plasma Mass Spectrometry analyses*

237 Elemental (major and trace elements, plus rare earth elements) analyses in twenty
238 samples, were also conducted using Inductively Coupled Plasma Mass Spectrometry (ICP-MS,
239 Agilent Technologies®) at the Water Quality Centre (Trent University, Canada), in
240 collaboration with the EnIGMA Research Laboratory.

241 Approximately 0.15 g of each sample was weighed in duplicate for REE+Y
242 determination and digested with 8 mL of *aqua regia* (HCl:HNO_3, 3/1, v/v). All acids were
243 previously double-distilled. Following pre-digestion (30 minutes), the samples were digested
244 on a hot plate at 120°C for 8 h. After cooling, the digests were transferred to 50 mL falcon
245 tubes and brought to a 12 mL with 2% HNO_3. The resulting solutions were subsequently diluted

150-fold with 2% HNO_3 in 15 mL falcon tubes prior to ICP-MS analysis. Analytical quality control was assessed using OREAS-46. Instrumental accuracy was further evaluated using SLRS-6, a certified reference material provided by National Council of Canada (NRC). The analytical results obtained for the certified reference materials are presented in the Supplementary Material 2.

To verify all possible chemostratigraphic correlations, the ΣREE+Y, ΣHREE, ΣLREE, ΣLREE/ΣHREE and the Y/Ho ratios were calculated to evaluate the correspondence among these stratigraphic layers. REE are particularly useful for chemostratigraphic studies because they can record subtle environmental changes, which make them valuable not only for chemostratigraphic correlation but also for assessing fossil transport. In general, the greater the geochemical difference between a fossil bone and its surrounding sedimentary matrix, the more likely it is that the fossil was transported before its final burial (Suarez et al., 2007; Guo et al., 2007; Kowal-Linka et al., 2014; Booth et al., 2025; Paim et al., 2025).

3.1.3. X-ray diffraction (XRD) analyses

X-ray diffraction (XRD) analyses were performed using a Malvern Panalytical (The Netherlands) AERIS benchtop X-ray diffractometer equipped with a Ni filter in the diffracted beam and operated at 30 kV and 10 mA using Cu Kα radiation (λ = 1.54178 Å). Diffraction patterns were collected over the angular range of 15–80° (2θ). Data were acquired with a step size of 0.043° (2θ) and a counting time of 100 s per step, using a 1/4° divergence slit, 0.04 rad Soller slits, a 23 mm mask, and the sample spinner enabled. A PIXcel 1D solid-state detector was employed.

Crystalline phases were identified based on the observed diffraction peak interplanar spacings (*d-spacings*) by comparison with the ICDD (International Centre for Diffraction Data)

database. Semiquantitative phase analysis was performed using the Reference Intensity Ratio (RIR) method (Hubbard and Snyder, 1988).

3.2. Statistical analysis

To establish the chemostratigraphy correlations among the five outcrops of the Crato Formation, this study employed the Hierarchical Cluster Analysis (HCA) using the Past 3.14 Software (Hammer et al., 2001) with data normalization by Ward's method (Ward, 1963). The HCA is a common method in data mining and statistics that seeks to build hierarchical clusters by an agglomerative ("bottom-up" approach; each data point is an individual cluster) or divisive ("top-down" approach; all data points start in a single cluster and recursively splits the cluster into smaller ones) ways (Nielsen, 2016). This method is particularly suitable for chemostratigraphic studies because it allows the objective grouping of samples based on multivariate geochemical similarities, enabling the recognition of chemically homogeneous stratigraphic units and supporting stratigraphic correlations between outcrops (e.g., Templ et al., 2008; Montero-Serrano et al., 2010).

3.3. Normalization of trace elements

To enable comparisons of our data with those from other localities and detect slight variations in the behavior of the chemical elements in different samples, we normalized the obtained concentrations against the distribution of the elements in the earth's crust (here named DEEC) proposed by Turekian and Wedepohl (1961), as well as against PAAS - Post-Archean Australian Average Shale (Nagarajan et al., 2007) standards. REE and Y contents were normalized by the C1 chondrite (Anders and Grevesse, 1989). Although Y has an ionic radius and geochemical behavior similar to those of the HREE (see Shannon, 1976), in this work, it was placed on the graphs after Lu to facilitate comparison with the behavior of the other REE.

This procedure resulted in a characteristic diagram known as the distribution pattern, which displays normalized elemental concentrations as a function of atomic number. Normalization is necessary because elements with even atomic numbers are generally more abundant than the odd ones, a phenomenon that produces a characteristic zig-zag pattern in the geochemical distribution diagrams, which is called Oddo-Harkins Effect. So, this normalization was applied to reduce or eliminate this zig-zag effect, allowing for clearer visualization and comparison of elemental distributions (e.g., Grawunder and Merten, 2011). In addition, it is a well-established standard in geochemical studies involving limestones (e.g., Nagendra et al., 2011; Chen et al., 2014). To verify the existence of relative enrichment or depletion of an element in each sample, we compared their contents with those existing in these standards. The enrichment (or depletion) condition was established when this pattern occurred in both standards (DEEC and PAAS). It is worth noting that the DEEC corresponds to an average compositional analysis in different types of rocks (from igneous to sedimentary). However, in this work, only the carbonates with sedimentary origin had their composition adopted.

3.4. Enrichment factor

Enrichment Factors (EF) were adopted to detect paleoenvironmental changes in the depositional process of the Crato Formation. EFs used either Fe or Al as normalizers, since both are mostly present within detrital minerals, like silica, phyllosilicates, plagioclases, and K-feldspars (Montero-Serrano et al., 2010; Rodríguez-Cuicas et al., 2019). The EF are determined through the following equation 1:

$$EF_{element} = \frac{([X]_{sample} / [Fe, Al]_{sample})}{([X]_{DEEC} / [Fe, Al]_{DEEC})} \quad (1)$$

where the $(X)_{Sample}$ and $(X/Fe, Al)_{Sample}$ correspond to the values obtained in the samples, and $(X)_{DEEC}$ and $(X/Fe, Al)_{DEEC}$ are associated with the average concentration found in the DEEC (Turekian and Wedepohl, 1961).

The use of Fe as a normalizer is highly effective for carbonates. Also, Fe content in the analyzed samples is higher than the Al's, improving EF interpretations. However, using Fe as the normalizing element has some limitations, especially in settings where diagenesis may have mobilized metals. But this does not seem to be the case in the laminated limestones of the Crato Formation (Hamid et al., 2024b). To address this issue, we also applied the Al as a normalizer (see Equation 1), due to its high stability, being conservative in the Earth's crust (Reimann and de Caritat, 1998; Merli et al., 2020). This approach has been successfully employed by previous studies in the Crato Formation that suggested that Fe in carbonatic phases originates from weathering and erosion processes rather than diagenetic processes (Heimhofer et al., 2010; Hamid et al., 2024b).

4. Results

4.1. Geochemical outcrop characterization

The most relevant element concentration averages that enabled the distinguishing of the five "*Talhados*" studied are summarized in Table 1. Individual sample concentrations are listed Supplementary Material 2 (S2) and summarized in Figure 2.

Table 1 - Average element contents (ppm) in the "*Talhados*" from the Crato Formation. The highest contents are in bold and the lowest, in italics. TJT = Talhado de Joaquim Teles; TW1 = Talhado de Wellington 1; TW2 = Talhado de Wellington 2; TT = Talhado de Tico Sisnando and MT = Mina da Tatajuba.

343

344 **Table 1**

345 **Table 1 -** Average element contents (ppm) in the "*Talhados*" from the Crato Formation. The
346 highest contents are in bold and the lowest, in italics. TJT = Talhado de Joaquim Teles; TW1
347 = Talhado de Wellington 1; TW2 = Talhado de Wellington 2; TT = Talhado de Tico Sisnando
348 and MT = Mina da Tatajuba.

349

Quarry	Al	Ti	V	Mn	Fe	Ni	Cu	Zn	Sr	Ba	Pb
TJT	3159	42	**14**	*1521*	7092	7	**205**	**683**	**916**	61	201
TW1	**3790**	**44**	13	2059	9501	**11**	137	653	682	**240**	*149*
TW2	3340	45	11	2181	**9614**	6	200	487	687	*42*	**220**
TT	2574	33	**14**	1734	6419	8	124	627	734	106	171
MT	*2133*	*27*	*10*	**2212**	*3840*	*4*	*74*	*521*	*662*	*78*	*119*

350

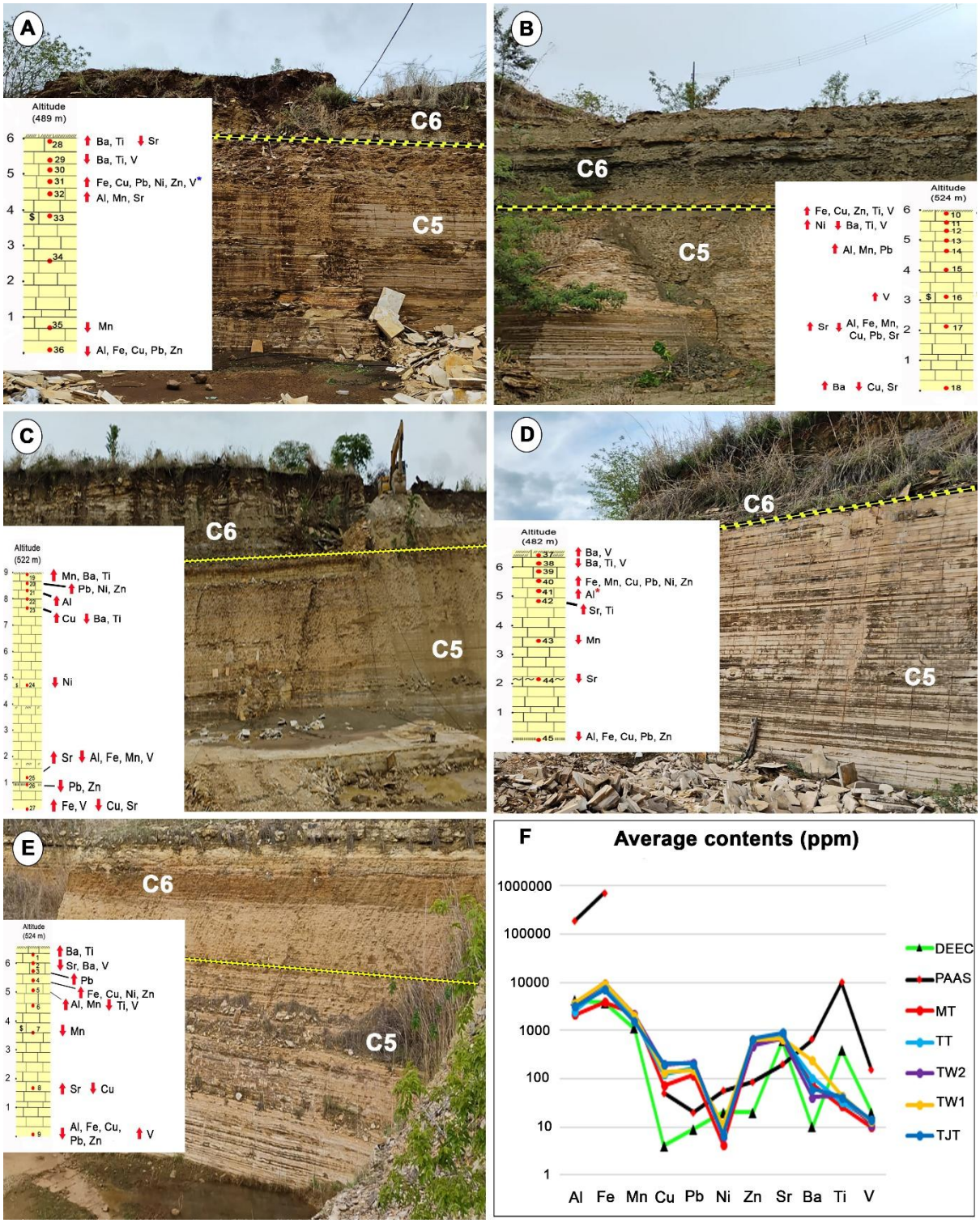

Figure 2

It seems that exists a trend of concentration of higher contents of Al, Mn, Fe, Zn and Pb near to the top of the exposed sections (close to the "Matracão" layer), whereas the lowest values tend to be recorded near their bottoms (near or within the "Lajão dos Sete Cortes" layer).

Therefore, the average contents of these elements may be used to distinguish the studied quarries (Table 1). The other elements, however, showed no consistent or distinctive pattern among the different "*Talhados*".

Based on the ICP-MS analyses, ΣREE+Y, ΣLREE, ΣHREE, ΣLREE/ΣHREE, and Y/Ho ratios were calculated (see Table S4). Among the samples, TJT4 exhibits the highest concentrations of most REE, whereas TT5 shows the lowest concentrations of all REE. The highest value of Y (14 ppm) was recorded in sample TT3. These geochemical patterns allow discrimination not only of the individual layers but also of the quarries from which they were collected.

Based on the average REE and Y concentrations, the studied quarries can be characterized as follows: TW1 exhibits the highest average values of La and Ce, whereas TT is enriched in Pr, Sm, Eu, Gd, Dy, Ho, Er and Y. In contrast, TW2 displays the lowest average concentrations of Er and Y, while MT exhibits the lowest of La, Ce, Pr, Sm, Eu, Gd, Tb and Dy. Additional details are provided in Table S4.

Based on the XRD analyses of 15 samples, the identified crystalline phases are presented in Table 2. All XRD patterns are provided in the Supplementary Material (Table S5).

Table 2 - Identification and semiquantitative analysis of the crystalline phases detected in each selected sample. **1** = $CaCO_3$ (ICDD 01-072-1652); **2** = SiO_2 (ICDD 01-079-1906); **3** = KCl (ICDD 00-004-0587).

Sample	Mineral Phases (%)		
	Calcite[1]	Quartz[2]	Sylvite[3]
TJT 2	99	1	-
TJT 3	99	1	-
TJT 4	99	1	-

TW1 2	98	1	1
TW1 3	99	1	-
TW1 4	99	1	-
TW2 2	99	1	-
TW2 3	98	2	-
TW2 4	98	2	-
TT2	99	1	-
TT3	99	1	-
TT4	99	1	-
MT2	100	-	-
MT3	98	2	-
MT4	99	1	-

Table 2

4.2. Normalization results

After normalizing the elemental concentration from the "*Talhados*", it was possible to identify those consistently enriched relative to both standards, whereas others are depleted. Elements such as Zn and Pb are enriched in almost all "*Talhados*", with only few exceptions (see Table 3). When the average geochemical composition of these strata is considered, this general pattern is maintained, with the additional consistent enrichment in Cu and Sr (see Tables 4 and S4).

Table 3 - Enrichment conditions (sample-by-sample observations) of the selected "*Talhados*" (Pedra Cariri quarries of the Crato Formation) compared with DEEC (Turekian & Wedepohl, 1961) and PAAS (Nagarajan et al., 2007) standards. An element is considered enriched or depleted when this pattern is observed in all the analyzed strata from the same quarry. Elements enriched relative to both standards (DEEC and PAAS) are shown in bold, whereas depleted elements are shown in italics. TJT = Talhado de Joaquim Teles; TW1 = Talhado de Wellington 1; TW2 = Talhado de Wellington 2; TT = Talhado de Tico Sisnando and MT = Mina da Tatajuba.

Quarry	DEEC		PAAS	
	Enriched	**Depleted**	**Enriched**	**Depleted**
TJT	**Zn**, **Sr** and **Pb**	*Al*, *Ti*, *V*, *Fe* and *Ba*	Cu, **Zn**, **Sr**, Ba and **Pb**	*Ti* and *V*
TW1	**Zn** and Sr	*Al*, *Ti*, *V*, *Fe* and *Ni*	Cu, **Zn**, Ba and Pb	*Ti* and *Ni*
TW2	Sr	*Al*, *Ti*, *V*, *Fe*, *Ni* and *Ba*	Cu, Zn and Ba	*Ti* and *Ni*
TT	**Zn**, **Sr** and **Pb**	*Al*, *Ti*, *V*, *Fe*, *Ni* and *Ba*	Cu, **Zn**, **Sr**, Ba and **Pb**	*Ti* and *Ni*
MT	**Zn**, Sr and **Pb**	*Al*, *Ti*, *V*, *Fe*, *Ni* and *Ba*	Cu, **Zn**, Ba and **Pb**	*Ti* and *Ni*

Table 3

Table 4 - Enrichment condition of the average geochemical content of the selected "*Talhados*" compared with DEEC (Turekian & Wedepohl, 1961) and PAAS (Nagarajan et al., 2007). Calculations are based on the average geochemical composition of each "*Talhado*". Elements enriched relative to both standards (DEEC and PAAS) are shown in bold, whereas depleted elements are shown in italics. TJT = Talhado de Joaquim Teles; TW1 = Talhado de Wellington 1; TW2 = Talhado de Wellington 2; TT = Talhado de Tico Sisnando and MT = Mina da Tatajuba.

Quarry	DEEC		PAAS	
	Enriched	**Depleted**	**Enriched**	**Depleted**
TJT	Fe, Mn, **Cu**, **Pb**, **Zn**, **Sr** and Ba	*Al*, *Ti*, *V* and *Ni*	**Cu**, **Zn**, **Sr** and **Pb**	*Al*, *Ti*, *V*, Fe, *Ni* and Ba
TW1	Fe, Mn, **Cu**, **Pb**, **Zn**, **Sr** and Ba	*Al*, *Ti*, *V* and *Ni*	**Cu**, **Zn**, **Sr** and **Pb**	*Al*, *Ti*, *V*, Fe, *Ni* and Ba
TW2	Fe, Mn, **Cu**, **Pb**, **Zn**, **Sr** and Ba	*Al*, *Ti*, *V* and *Ni*	**Cu**, **Zn**, **Sr** and **Pb**	*Al*, *Ti*, *V*, Fe, *Ni* and Ba
TT	Fe, Mn, **Cu**, **Pb**, **Zn**, **Sr** and Ba	*Al*, *Ti*, *V* and *Ni*	**Cu**, **Zn**, **Sr** and **Pb**	*Al*, *Ti*, *V*, Fe, *Ni* and Ba
MT	Fe, Mn, **Cu**, **Pb**, **Zn**, **Sr** and Ba	*Al*, *Ti*, *V* and *Ni*	**Cu**, **Zn**, **Sr** and **Pb**	*Al*, *Ti*, *V*, Fe, *Ni* and Ba

Table 4

Based on the information, summarized in Figures 3 and 4 and Tables 3, 4 and S4, Ti is the only element that presents a contrasting behavior within both standards. It is depleted within all the analyzed strata in comparison with DEEC and PAAS.

When the average geochemical composition of these quarries is considered, Cu, Zn, Sr and Pb are enriched relative to both the DEEC and PAAS standards, whereas Al, Ti, V and Ni are depleted in all mines. These results are summarized in Tables 4 and S4.

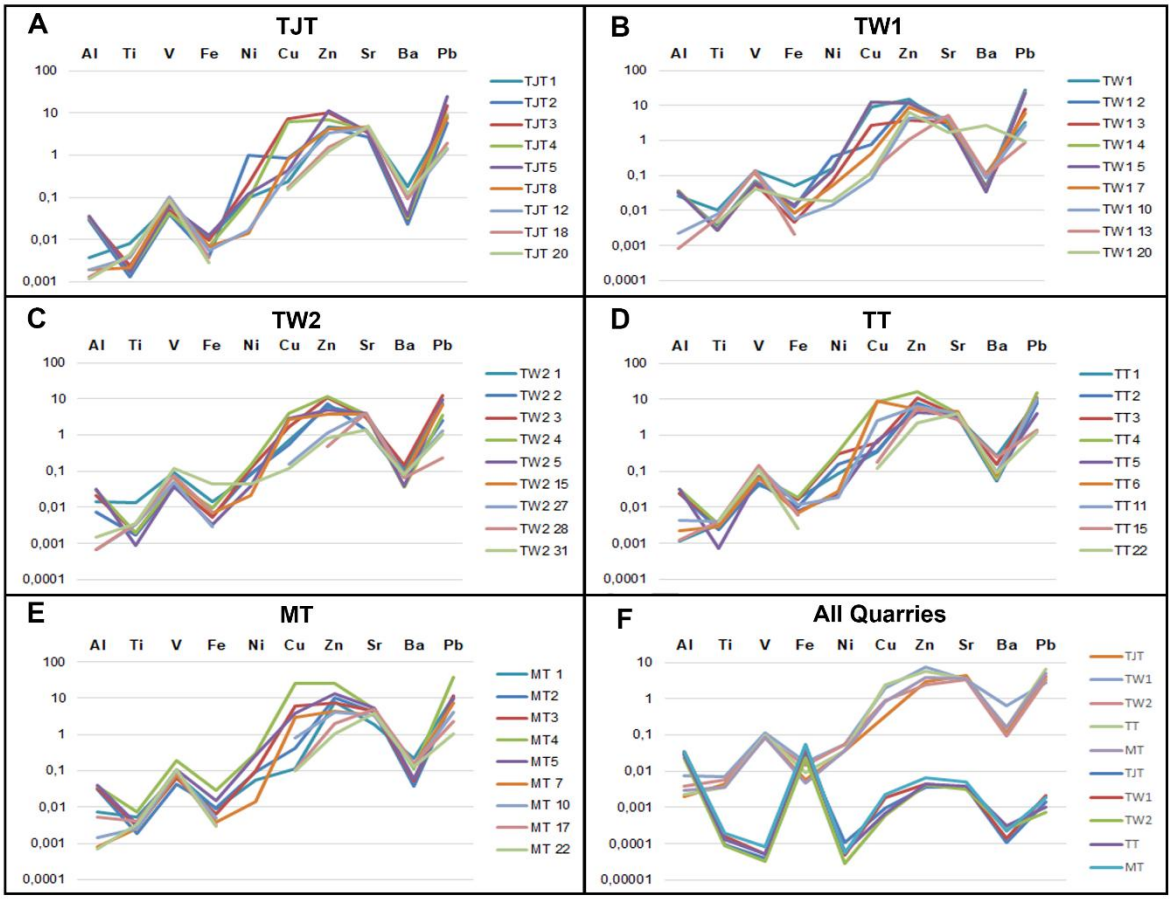

419

420 **Figure 3**

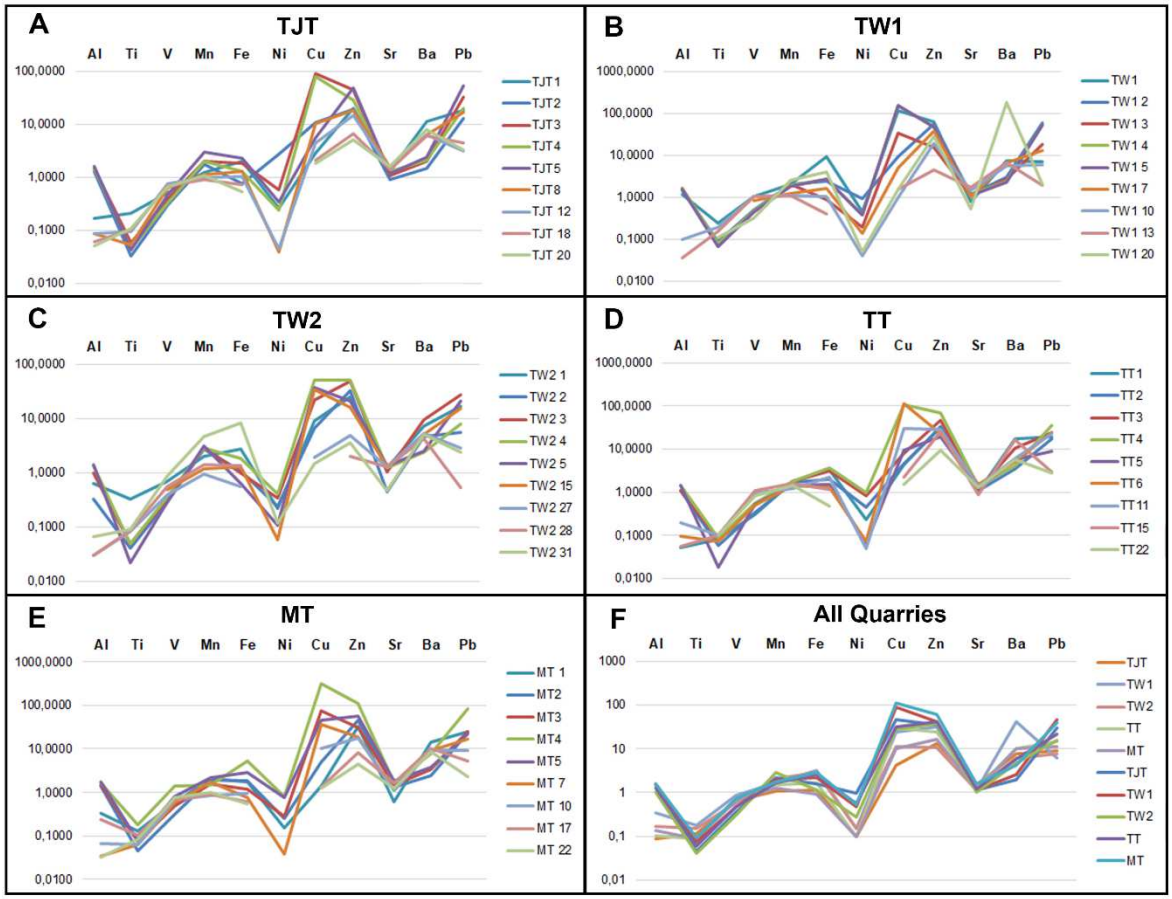

Figure 4

After normalizing the REE and Y concentrations to C1 Chondrite (Anders and Grevesse, 1989), the normalized patterns reveal a progressive depletion from LREE to HREE across all the studied quarries (Table S4). Overall, the quarries are enriched in REE and Y relative to C1 Chondrite, except for Lu, which is consistently depleted in all quarries (Table S4).

4.3. Chemical statistical correlation

Following the principles of HCA (Ward, 1963; Murtagh and Contreras, 2012; Nielsen, 2016), the analyses identified two main clusters: one including Talhado de Tico Sisnando (TT) and Talhado de Joaquim Teles (TJT), and another comprising Talhado de Wellington 1 and 2 (TW1 and TW2; Fig. 5A). Mina da Tatajuba (MT) forms a separate group (Fig. 5A).

433 Hierarchical clustering based on REE concentrations (20 samples) also revealed two main
434 clusters: one encompassing Talhado de Wellington 2 (TW2) and Mina da Tatajuba (MT), and
435 other comprising Talhado de Wellington 1 and Talhado de Joaquim Teles (TW1 and TJT; Fig.
436 5B). In this analysis, the Talhado de Tico Sisnando (TT) is closely associated with the latter
437 cluster.

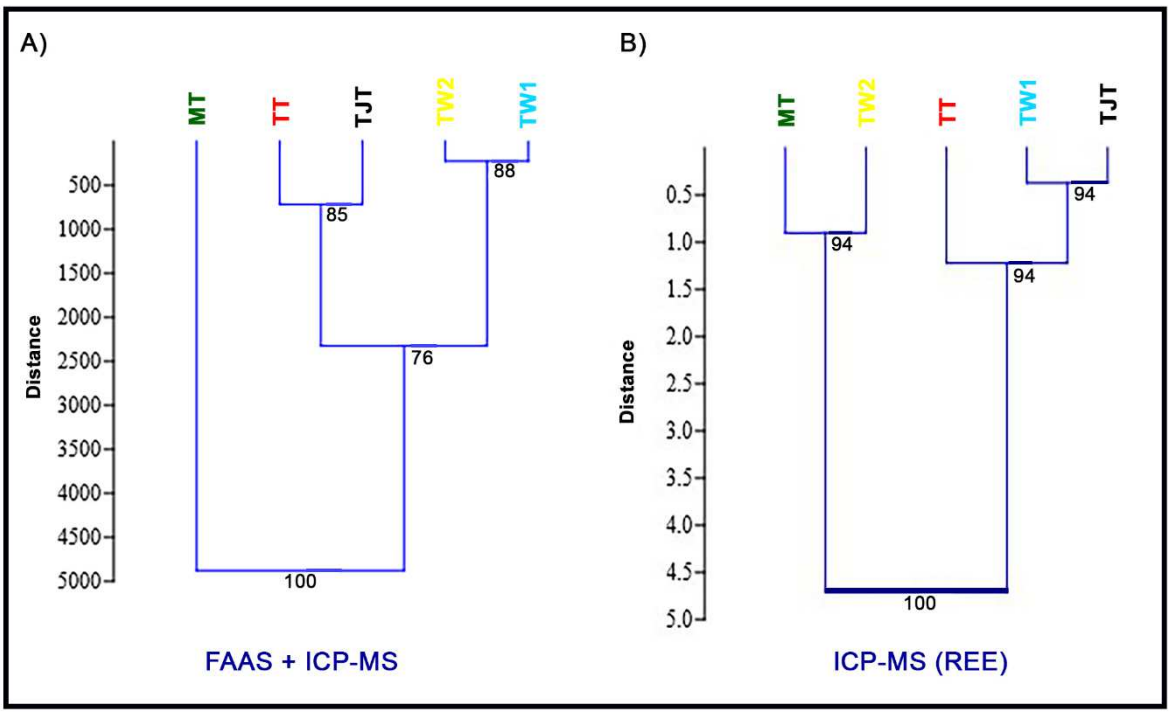

438

439

440 **Figure 5**

441

442 **4.4. Enrichment Factor (EF)**

443 Most of the highest EF_{Fe} values were detected in Mina da Tatajuba (MT), highlighting
444 the values of Mn (1.99), Zn (25.76) and Pb (13.14). Most of the lowest EF values were observed
445 in Talhado de Wellington 2 (TW2), emphasizing Zn (9.63) and Ba (1.64). It is worth
446 mentioning that the highest EF_{Fe} values are more distinguishable than the lowest ones, thus are
447 more reliable for quarry characterization (Table 5). For the EF_{Al}, most of the highest values
448 were observed in Talhado de Tico Sisnando (TT) and Mina da Tatajuba (MT), highlighting the

449 values of Fe (3.38), Zn (51.26) and Pb (31.09). Most of the lowest EF_{Al} values were observed
450 in Talhado de Wellington 1 and 2 (TW1 and TW2), particularly those of V (0.68), Sr (1.24)
451 and Ba (5.22; Table 5).

452 **Table 5 -** Fe and Al enrichment factors (EF) of the selected "*Talhados*" compared with values
453 reported in the literature. Highest EFs are shown in bold, whereas the lowest are in italics. 1 =
454 Fathy et al. (2021); 2 = Du et al. (2025); 3 = Hamid et al. (2024b). The red dashed line splits
455 the data of this study with those from the literature. TJT = Talhado de Joaquim Teles; TW1 =
456 Talhado de Wellington 1; TW2 = Talhado de Wellington 2; TT = Talhado de Tico Sisnando
457 and MT = Mina da Tatajuba.

Quarries	Enrichment Factor (EF_{Fe})										
	Al	**Ti**	**V**	**Mn**	**Fe**	**Ni**	**Cu**	**Zn**	**Sr**	**Ba**	**Pb**
TJT	0.40	0.06	0.37	*0.74*	1.00	0.19	**27.48**	18.29	0.80	3.28	11.95
TW1	0.36	0.04	0.26	0.75	1.00	**0.23**	*13.68*	13.07	*0.45*	**9.61**	*6.63*
TW2	0.31	0.04	*0.21*	0.78	1.00	*0.13*	19.76	*9.63*	*0.45*	*1.64*	9.67
TT	*0.30*	0.04	0.34	0.76	1.00	0.18	14.96	15.16	0.58	5.12	9.21
MT	**0.50**	**0.07**	**0.50**	**1.99**	1.00	0.22	18.26	**25.76**	**1.07**	7.69	**13.14**
1	**2.01**	**0.97**	0.68	0.02	1.00	0.13	0.48	-	0.02	0.01	-
2	1.40	0.72	0.60	0.08	1.00	0.19	0.89	0.88	0.61	8.71	0.26
3	-	-	**8.00**	**13**	1.00	**7.00**	**209**	**90**	-	3.00	**133**
Quarries	**Enrichment Factor (EF_{Al})**										
	Al	**Ti**	**V**	**Mn**	**Fe**	**Ni**	**Cu**	**Zn**	**Sr**	**Ba**	**Pb**
TJT	1.00	**0.14**	0.92	*1.84*	2.48	0.46	68.20	45.38	2.00	8.14	29.64
TW1	1.00	*0.12*	0.71	2.07	2.77	**0.64**	37.89	36.20	*1.24*	**26.62**	*18.37*
TW2	1.00	**0.14**	*0.68*	2.49	3.18	*0.41*	**62.87**	*30.65*	1.42	*5.22*	30.78
TT	1.00	0.13	**1.14**	2.57	**3.38**	0.61	50.51	51.18	1.96	17.28	**31.09**
MT	1.00	0.13	0.99	**3.96**	*1.99*	0.43	*36.32*	**51.26**	**2.14**	15.30	26.14
1	1.00	**0.51**	0.43	0.06	0.71	0.13	0.64	*0.63*	0.43	6.21	*0.18*
2	1.00	0.48	0.34	*0.01*	*0.50*	*0.07*	*0.24*	-	*0.01*	*0.27*	-
3	-	-	**16**	**22**	2.00	**13**	**385**	**156**	-	5.00	**213**

458

459

460 **Table 5**
461

462 **5. Discussion**

463 **5.1. Enrichment Factor (EF) and Hierarchical Cluster Analysis (HCA)**

Comparing the EF_{Fe} data from Table 5 with those calculated from previous studies (Fathy et al., 2021; Du et al., 2025) it was possible to verify that EF_{Fe} for Al, Ti, V, Mn, Ni, Cu, Zn and Pb are higher in the reviewed literature than in the quarries analyzed from the Crato Formation. In contrast, Sr and Ba have higher EF_{Fe} values in the studied quarries compared to those observed in the literature, which can help to distinguish these units. The EF_{Fe} for Sr and Ba, calculated based on Du et al. (2025) data (0.61 and 8.71, respectively), are higher than in most of the studied mines, except for Sr in TJT (0.80) and MT (1.07), and Ba in TW1 (9.61). These preliminary results suggested that the analyzed quarries can be differentiated from other Cretaceous units in Egypt and China. This information is summarized in Fig. 6. It is worth noting that the Quseir Formation in Egypt, although an Upper Cretaceous unit, is the geographically closest African analogue. It represents lacustrine, organic-rich deposits that are likely comparable to those proposed for the Crato Formation and, importantly, it provides geochemical data from which enrichment factors (EF) can be calculated. The Madongshan Formation in China, by contrast, is geographically distant but of similar age (Aptian), offering another useful point of comparison.

The EF_{Al} values presented in Table 5 suggest that the "*Talhados*" of the Crato Formation generally exhibit higher EF values than those reported in the literature, except for the EF_{Al} of Ti (0.51 and 0.48), which can also be used to differentiate these units. Particular attention should be given to the Talhados de Tico Sisnando (TT) and the Mina da Tatajuba (MT), which show most of the highest EF_{Al} values among the studied "*Talhados*". In addition, since Al is considered one of the most immobile elements in the Earth's crust (Reimann and de Caritat, 1998; Merli et al., 2020), these EF_{Al} can be regarded as more reliable than those calculated using Fe as a normalizer (EF_{Fe}).

Based on the enrichment factors (EF_{Fe} and EF_{Al}) calculated from the data of Hamid et al. (2024b), which were obtained from a "*Talhado*" (Talhado de Antônio Finelon) located

within the same quarry area as TW1 and TW2 in this study, it was possible to note substantial differences between their EF values and those reported here (Table 5; Fig. 6). Considering that these "*Talhados*" belong to different facies (respectively C6 and C5) and are geographically close, such large EF contrasts may, at least preliminarily, reflect variations in the depositional conditions. This observation probably suggests that the Crato Formation may not represent a single uniform water body but instead may have consisted of multiple sub basins or water masses, each with their own microenvironmental contexts.

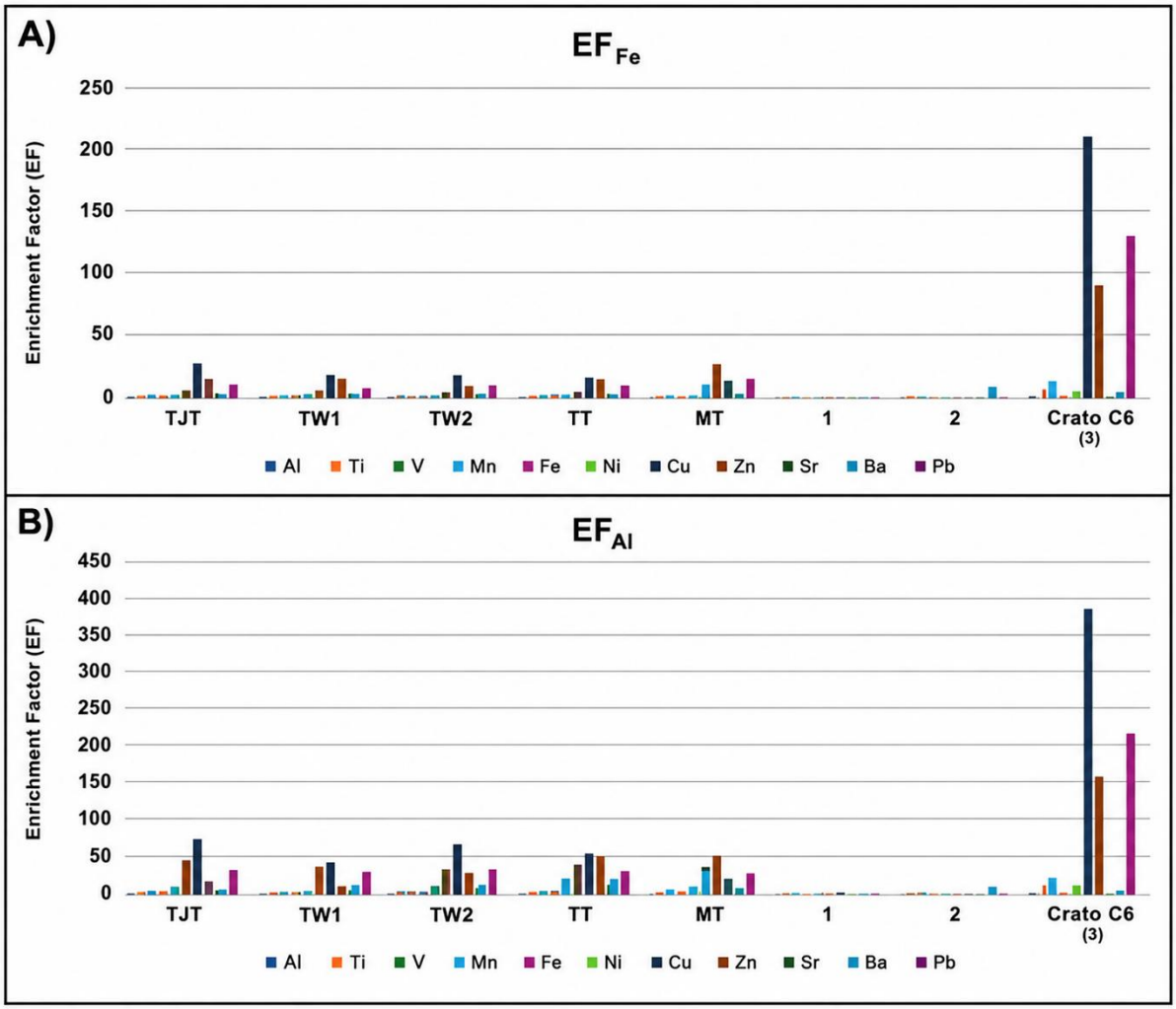

Figure 6

HCA analyses have been employed as a chemometric tool to characterize depositional environments of source rocks in Brazilian basins, including the Pimenteiras Formation

(Parnaíba Basin) and the Irati and Ponta Grossa formations (Paraná Basin; Garcia et al., 2020). According to those authors, the method is useful for distinguishing samples into discrete groups, thereby identifying intervals that contain mixtures of marine and terrestrial organic matter (i.e., transitional depositional settings). Another example of HCA application was reported for the Eocene Green River Formation (USA), where it was used to refine chemofacies characterization and to document fluctuations in lake chemistry (Wu et al., 2022). Here, two main clusters were found (Fig. 7), which suggest that the mines within each group can share similar depositional contexts and exhibit highly correlated geochemical signatures. Future studies should evaluate the differences between the HCA clusters obtained from the combined FAAS + ICP-MS dataset and those derived from the REE (ICP-MS) dataset (Fig. 5) to determine which dataset better discriminates the studied quarries.

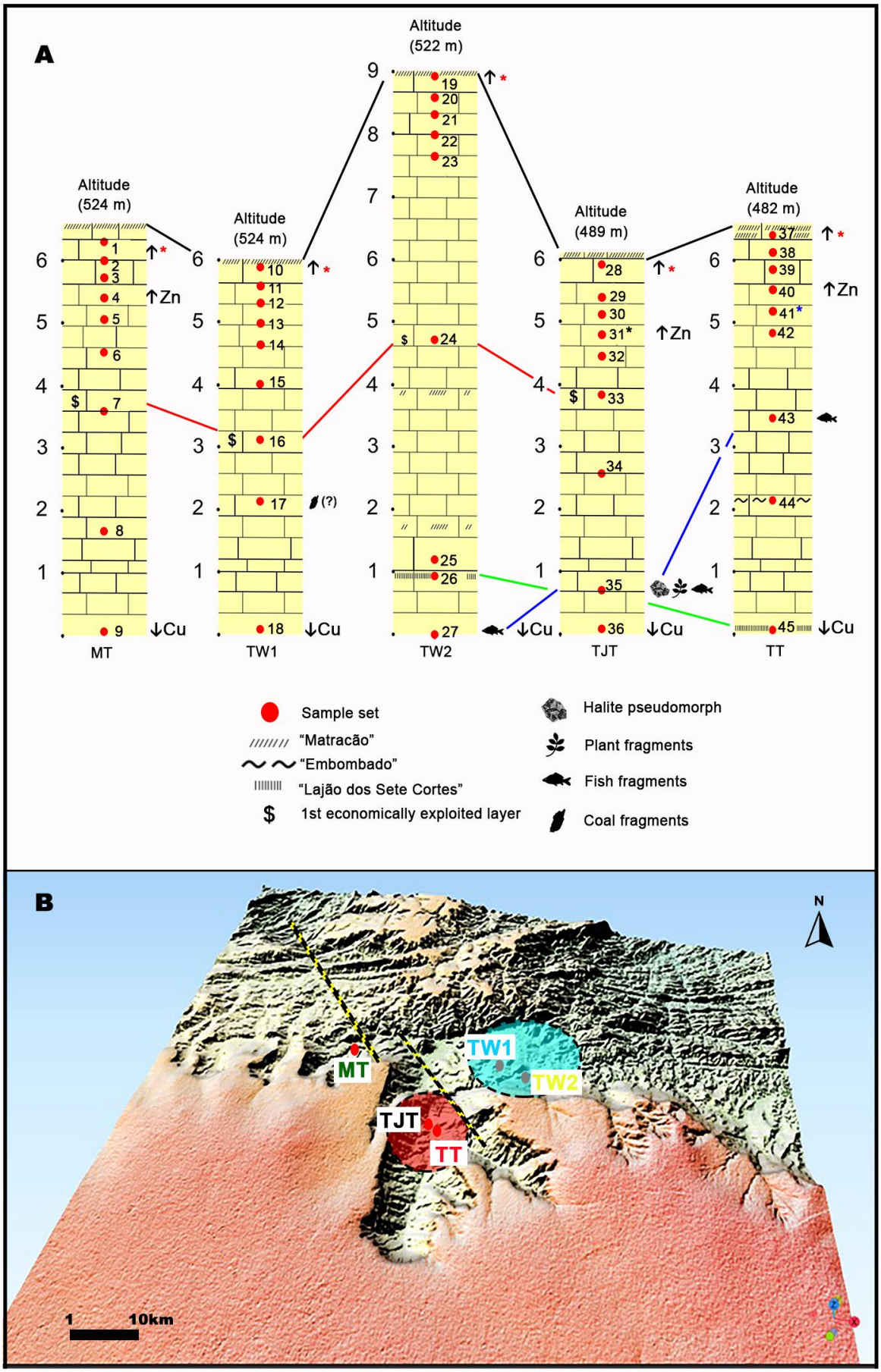
A
Altitude (524 m)
Altitude (524 m)
Altitude (522 m)
Altitude (489 m)
Altitude (482 m)
↑Zn
↓Cu
MT
TW1
TW2
TJT
TT
Sample set
"Matracão"
"Embombado"
"Lajão dos Sete Cortes"
1st economically exploited layer
Halite pseudomorph
Plant fragments
Fish fragments
Coal fragments
B
N
MT
TW1
TW2
TJT
TT
1
10km

514

515 **Figure 7**

516

517 **5.2. Chemostratigraphic and statistical correlations**

518 Major and trace elements have been used as tools for characterize the stratigraphy of
519 different depositional context and ages (e.g., Das, 1997; Fačevicová et al., 2016; Sial et al.,
520 2018; Fathy et al., 2021; Ravidà et al., 2023; Du et al., 2025), and in some studies in the Araripe
521 Basin (Corecco et al., 2022; Hamid et al., 2024a,b). Based on this study preliminary results, it
522 is possible to note that there is a tendency for higher concentrations in the uppermost layers
523 and lower in the lowermost ones (see Fig. 2 and Table S2). However, it seems that only the
524 lower contents of Cu, near the bottoms (near or within the "Lajão dos Sete Cortes" layer; see
525 Fig. 2 and 6C), can be used as a chemostratigraphic mark (index strata) for the Crato Formation.
526 These low Cu values seem to be associated with the lowermost C5 unit layers of the laminated
527 limestones (Fig. 7A). In addition, it is possible to associate paleontological and
528 ethnostratigraphic observations (Fig. 7A).

529 With slightly lower consistency, Ba and Ti (red stars in Fig. 7A) contents correlate
530 with the uppermost C5 unit layers in three of the five studied "*Talhados*", except in TW1,
531 where the red star represents only the Ti values and in TT, where it corresponds only to the Ba
532 contents. This pattern is more consistent with the preliminary HCA dendrogram shown in
533 Figure 5B, in which TW1 and TT cluster together as a sister group with 94% support. In
534 contrast, the dendrogram shown in Figure 5A also suggests these "*Talhados*" as sister groups,
535 although with lower support (76%). Nevertheless, additional analyses are required to confirm
536 this chemostratigraphic marker and the grouping suggested by the HCA.

537 Comparing the REE values obtained in this study with those reported for the lutites
538 from the Três Irmãos quarry, Crato Formation, by Salgado-Filho et al. (2021), it is possible to

observe a trend towards LREE enrichment relative to HREE in both datasets. Despite this similarity, both ΣLREE (77.8–245) and ΣHREE (9.6–28.5) values in the lutites are much higher than those detected in this study (13.1–45.3 and 0.6–1.9, respectively). In addition, the samples analyzed by Salgado-Filho et al. (2021) show positive Eu anomalies and negative Gd anomalies, which is opposite to the pattern observed in the samples analyzed in this study, at least for Gd. These differences may be related to the contrasting lithologies represented by the two sample sets (lutites and laminated limestones), which may reflect distinct depositional contexts. Another possible comparison is between the REE values obtained in this study and those reported for the laminated limestones of the C6 unit (Hamid, unpublished data). Again, both datasets show a trend towards LREE enrichment relative to HREE. However, both ΣLREE (64.4–156.8) and ΣHREE (4.2–7.7) values detected in the C6 unit are considerably higher than those obtained in this study. Thus, the geochemical data allow the C5 unit to be distinguished not only from different lithologies, such as lutites and laminated limestones, but also from different facies within the Crato Formation, as represented by the C5 and C6 units. These findings reinforce the value of REE as chemostratigraphic proxies, as they can record subtle geochemical and environmental variations (Booth et al., 2025; Paim et al., 2025).

Comparing the DEEC- and PAAS-normalized results of this study (C5 facies; Table 4) with those calculated by Hamid et al. (2024b; C6 facies), it is possible to note that the C5 and C6 units are enriched in nearly the same elements (Cu, Zn, and Pb), except for Sr, which is enriched only in C5. Thus, C5 and C6 can be distinguished based on their Sr enrichment. Additionally, the C5 outcrops display vertical geochemical variations that allow differentiation of individual layers (Tables 1 and S2). These results indicate that normalization against DEEC and PAAS, together with the EF, can be used as an effective chemostratigraphic tool to distinguish not only between the C5 and C6 units, but also among individual C5 outcrops, highlighting the relevance of this approach for intra-unit stratigraphic discrimination.

564 Considering the strong positive correlations (> 0.9) observed when the calculations
565 were made within the individual "*Talhados*", the samples of each "*Talhado*" seem to correlate
566 among each other. However, regarding all the samples analyzed, these correlations decrease
567 with the high values in order of 0.7 (Table S3). It is worth mentioning the strong negative
568 correlations (-0.9) observed in TW2 (Sr-Fe = -0.937 and Sr-Mn = -0.968) and MT (V-Mn = -
569 0.968). The correlations, however, must be interpreted with attention, since these values can
570 be related to some of these reasons: high standard deviation (SD > 20), or dolomitization. The
571 high SD increases the likelihood of underestimating true correlations and the influence of
572 extreme values (Hinkle et al., 2003; Schober et al., 2018). On the other hand, the dolomitization
573 process during diagenesis, commonly enriches Mn and Fe in carbonates and can alter the trace
574 elements associations (e.g., Mn/Sr, Fe-Mn-Sr) relative to the primary calcitic limestone (Brand
575 and Veizer, 1980; Banner and Hanson, 1990). Dolomitic phases were already reported for some
576 of the strata of the Crato Formation (Corecco et al., 2022). Despite this, no dolomitic phases
577 were identified in the samples analyzed in this study by XRD (Table 2). Therefore, both
578 hypotheses are plausible and require further investigation to determine the cause of these weak
579 statistical correlations. It is worth noting that, considering calcite is the most abundant mineral
580 phase detected in all the samples studied (Table 2), XRD analysis alone is not sufficient to
581 differentiate among the quarries visited.

582 Despite that, in general, each "*Talhado*" has its own characteristic geochemical
583 composition. In future studies, if the chemical compositions of the fossils from these
584 "*Talhados*" are similar to those of the carbonate rocks that host them, it will be possible to
585 identify the provenance of illegally traded fossils. However, this will require more detailed
586 investigations, including sampling of low interval carbonate layers within these "*Talhados*", in
587 order to achieve greater statistical significance.

588

589 **5.3. Tectonic interference in chemostratigraphic correlations**

590 A fault with NW-SE to WNW-ESE orientation was identified splitting MT, TJT and
591 TT "*Talhados*" and TW1 and TW2 (Fig. 7B). A tectonic and stratigraphic study recently
592 revealed that the Upper Jurassic and Lower Cretaceous evolution of the Araripe Basin, which
593 includes the Crato Formation, were related to the Gondwana breakup and strongly influenced
594 by intraplate stress propagation (Rosa et al., 2023). Two distinct reactivations of the
595 Precambrian Patos Shear Zone (PASZ) pre-existing basement structures were detected, which,
596 according to these authors, resulted in a paleostress inversion during basin's evolution.
597 The first of these reactivations, confined to the North by the PASZ and occurred
598 between the Jurassic to the Early Cretaceous affected the Brejo Santo, Missão Velha, and
599 Abaiara formations. It was associated with a set of normal to oblique NE-SW faults with
600 sinistral reactivation, forming a transtensional horsetails structure that controlled the initial
601 basin geometry. The second phase occurred along the Aptian post-rift stage and was
602 characterized by NE-SW reverse faults and a set of normal to oblique-normal faults striking
603 NW-SE to WNW-ESE. This fault arrangement generated a new NW-NE transtensional basin
604 that controlled the Barbalha Formation (Rosa et al., 2023). In this tectonic context, the observed
605 fault should be associated with the second reactivation phase of the PASZ. Despite that, more
606 detailed studies must be carried out to calculate this fault's rejection to better understand its
607 influence on these outcrops' deposition, and by consequence, in their geochemical signatures
608 and in their preliminary chemostratigraphic marks.
609 The results presented here indicate that fluctuations occurred in the input of chemical
610 elements among the different "*Talhados*", which is reflected in the low statistical correlations
611 observed when all sites are analyzed together. From a geochemical perspective, these variations
612 reveal differences in elemental behavior laterally (among the sampled outcrops) and vertically
613 (within individual "*Talhados*") across the laminated limestones of the Crato Formation. Such
614 compositional variability may reflect the existence of distinct source areas supplying elements

615 to different parts of the basin, as well as localized variations in the intensity of depositional or
616 post-depositional processes, leading to differential remobilization of chemical elements. These
617 geochemical patterns allow the discrimination of individual "*Talhados*" and suggest changes
618 in depositional conditions within the Crato paleolake, supporting the interpretation of multiple
619 microenvironments. Furthermore, these geochemical signatures may also be preserved within
620 the fossils of the C5 unit. As such, future studies should test this hypothesis by establishing
621 chemostratigraphic correlations between host rocks and their fossil content, providing a
622 valuable tool to recover lost fossil provenance data and to place illegally collected specimens
623 from the Araripe Basin back into their original stratigraphic context, thereby contributing to a
624 better understanding of this remarkable Cretaceous ecosystem.

625 **5.4. Chemostratigraphy as a tool for correlating fossils of unknown provenance**

626 As demonstrated here, the geochemical characterization of fossiliferous layers can
627 provide a valuable starting point for correlating fossils of unknown provenance. Multiproxy
628 analyses, particularly those based on ICP-MS data, including trace elements and rare earth
629 elements (REE), can detect subtle geochemical and environmental variations that may, in some
630 cases, serve as "tracking elements" or geochemical tracers for specific outcrops, as
631 demonstrated in this study. In addition, geochemical normalization against standard reference
632 patterns can also help distinguish different units within the basin and across different localities
633 (e.g., Corecco et al., 2020). In mineralogically monotonous or relatively homogeneous
634 geological contexts, such as those observed in the Araripe Basin, where calcite predominates
635 in all the analyzed layers, X-ray diffraction alone may not be sufficient to distinguish individual
636 outcrops.

637 Another important aspect highlighted by this study, which should be further
638 investigated, is the possibility of correlating fossils with their original stratigraphic layers.
639 However, caution is required because the hydroxylapatite comprising fossil bones can act as

sink for several chemical elements, including F, Sr, Pb, U, REE (Toledo and Pereira, 2001; Suarez et al., 2007; Paim et al., 2025). Consequently, perhaps the most reliable approach for correlating fossils of unknown provenance with their original layers or quarries may be to analyze their sedimentary matrices, thereby reducing the influence of fossil diagenetic effects. By doing so, chemostratigraphy may be further established as a useful tool for addressing this type of problem, particularly in the Araripe Basin, a region with a well-documented history of illegal fossil collection, which provides a relevant case study for this approach.

6. Conclusions

Based on the preliminary geochemical results presented here, there are variations in elemental behavior across the laminated limestones of the Crato Formation, both within individual "*Talhados*" (vertically) and among the different sampled sites (laterally). These observations suggest that the Crato Formation may not represent a single, uniform water body but rather, a system composed of multiple sub-basins or water masses, each with its own microenvironmental characteristics. At present, only two preliminary chemostratigraphic markers can be cautiously proposed among the studied quarries: low Cu contents for tracking the lowermost layers (near or within the "Lajão dos Sete Cortes") of the C5 facies and, with slightly lower consistency, Ba and Ti (red stars in Fig. 7A) elevated concentrations for tracking the upper C5 layers. The DEEC- and PAAS-normalized results also proved to be a useful tool for intra-unit stratigraphic discrimination. The NW–SE to WNW–ESE-oriented fault should be investigated further to evaluate its potential influence on the geochemical signatures of the "*Talhados*" and on the proposed chemostratigraphic markers (Ba, Ti and Cu). At this stage, the geochemical data suggest that the C5 unit can be differentiated not only from distinct lithologies, such as lutites and laminated limestones, but also from other depositional facies within the Crato Formation, as illustrated by the comparison between the C5 and C6 units.

These geochemical signatures may likewise be recorded in fossils from this unit. Future studies should evaluate this hypothesis by establishing chemostratigraphic correlations between fossil-bearing strata and the fossils themselves. This strategy has the potential to become an important tool for reconstructing lost provenance information and for reinserting illegally collected specimens from the Araripe Basin into their original stratigraphic positions, ultimately enhancing paleoenvironmental and paleoecological interpretations of this remarkable Cretaceous ecosystem.

Acknowledgements

L.C. thanks to the Conselho Nacional de Desenvolvimento Científico e Tecnológico - CNPq and to the Programa Institutos Nacionais de Ciência e Tecnologia - INCTPaleovert (#406902/2022-4 coordinated by A.W.A.K.) for his postdoctoral grant (#3153644/2024-9). I.H. thanks to the CNPq (#201162/2025-3) and to the Coordenação de Aperfeiçoamento de Pessoal de Nível Superior – Brasil (CAPES) – Financial code 001 (#88887.947184/2024-00). M.B.S thanks to the CNPq (#308515/2023-4) and Fundação de Amparo à Pesquisa do Estado do Rio de Janeiro -FAPERJ (#E-26/204.181/2024). A.W.A.K thanks to the CNPq (#406902/2022-4; #308707/2023-0) and Fundação Carlos Chagas Filho de Amparo à Pesquisa do Estado do Rio de Janeiro - FAPERJ (#E-26/200.558/2026). This work was also funded with resources from the INCT-TMCOcean - National Council for Scientific and Technological Development - CNPq Proc. No. 405.765/2022-3 and Ceará Foundation for Support to Scientific and Technological Development - FUNCAP Procs. Nos. ITR-0214-0010901.00/23. L.C. also thanks A. Bruch, for his assistance in the construction of the tectonic model used in Figure 7B.

References

689 Aldrich R (2009) Colonial museums in a postcolonial Europe. Afr Black Diaspora 2(2):137-
690 156

691 Anders E, Grevesse N (1989) Abundances of the elements: Meteoritic and solar. Geochim
692 Cosmochim Acta 53(1):197–214

693 Antonietto LS, Hamid I, Holgado B, Rocha AL, Ferreira MA, Saraiva AÁF, Lacerda LD, Silva
694 RC (2025) Reconstructing paleo-trophic relationships on the Brazilian Romualdo
695 Formation (Early Cretaceous) through mercury analysis in fossils. Front Earth Sci
696 13:1551085

697 Araújo-Júnior HI (2023) On repatriation of Brazilian fossil specimens. Derbyana 44:e805

698 Araújo-Júnior HI, Ghilardi RP, Caminha SAFS, Ribeiro VR, Barbosa FHS, Scheffler SM,
699 Ribeiro AM (2024a) Designation as cultural heritage best protects Brazilian fossils. Nat
700 Ecol Evol 8:1052–1053

701 Araújo-Júnior HI, Ghilardi RP, Ribeiro VR, Ribeiro AM, Barbosa FHS, Negri FR, Scheffler
702 SM (2024b) Scientific societies have a part to play in repatriating fossils. Nat Ecol Evol
703 8(3):355–358

704 Assine ML (2007) Bacia do Araripe. Bol Geociênc Petrobras 15(2):371-389

705 Assine ML, Perinotto JAJ, Custódio MA, Neumann VH, Varejão FG, Mescolotti PC (2014)
706 Sequências deposicionais do Andar Alagoas da Bacia do Araripe, Nordeste do Brasil.
707 Bol Geociênc Petrobras 22(1):3–28

708 Banner JL, Hanson GN (1990) Calculation of simultaneous isotopic and trace element
709 variations during water-rock interaction, with applications to carbonate diagenesis.
710 Geochim Cosmochim Acta 54:3123–3137

711 Batista MEP, Saraiva AÁF, Lima FJ, Bantim RAM, Pinheiro AP, Silva DB, Kunzmann L
712 (2024) An enigmatic tropical conifer from the Early Cretaceous of Gondwana. Acta
713 Palaeontol Pol 69(3):375–393

714 Benigno APA, Saraiva AÁF, Sial AN, Lacerda LD (2021) Mercury chemostratigraphy as a
715 proxy of volcanic-driven environmental changes in the Aptian–Albian transition, Araripe
716 Basin, northeastern Brazil. J S Am Earth Sci 107:103020

717 Bezerra FI, Solórzano-Kraemer MM, Mendes M (2021) Distinct preservational pathways of
718 insects from the Crato Formation, Lower Cretaceous of the Araripe Basin, Brazil. Cretac
719 Res 118:104631

720 Bom MHH, Ceolin D, Kochhann KGD, Krahl G, Fauth G, Bergue CT, Savian JF, Strohschoen
721 Júnior O, Simões MG, Assine ML (2021) Paleoenvironmental evolution of the Aptian
722 Romualdo Formation, Araripe Basin, Northeastern Brazil. Global Planet Change
723 203:103528

724 Booth S, Snyder K, Chadwick A, Ash RD, Voegele KK, Ullmann PV (2025) Rare Earth
725 Element Concentrations as a Novel Proxy for Lateral Continuity: An Initial Case Study
726 in the Cretaceous Lance Formation of Wyoming. Minerals 15(9):919

727 Brand U, Veizer J (1980) Chemical diagenesis of a multicomponent carbonate system—1:
728 Trace elements. J Sediment Petrol 50:1219–1236

729 Brasil (1942) Decreto-Lei nº 4.146, de 4 de março de 1942. Dispõe sobre a proteção dos
730 depósitos fossilíferos. https://www.planalto.gov.br/ccivil_03/decreto-lei/1937-
731 1946/del4146.htm. Accessed 15 Feb 2025

732 Campos APC, De Carvalho RT, Straker LC, Salgado LT, Kellner AWA, Farina M (2019)
733 Combined microscopy and spectroscopy techniques to characterize a fossilized feather
734 with minimal damage to the specimen. Micron 120:17–24

735 Castro R, Santos-Silva T, Fambrini G, Souza Neto JA, Pereira R (2017) Caracterização
736 geoquímica de folhelhos betuminosos da Formação Ipubi, bacia do Araripe, NE Brasil.
737 Geochim Bras 31(1):11–27

738 Cerri RI, Warren LV, Assine ML (2024) Source-to-sink reconstruction of early Paleozoic
739 Western Gondwana mega-scale alluvial systems. Earth-Sci Rev 258:104940

740 Chen S, Gui H, Sun L (2014) Geochemical characteristics of REE in the Late Neo-proterozoic
741 limestone from northern Anhui Province, China. Chin J Geochem 33(2):187–193

742 Cheng X, Kellner AWA, Saraiva AÁF (2018) The largest flying reptile from the Crato
743 Formation, Lower Cretaceous, Brazil. Hist Biol 32(3):321–329

744 Cisneros JC, Raja NB, Ghilardi AM, Dunne EM, Pinheiro FL, Fernández ORR, Sales MAF,
745 Rodríguez-de la Rosa R, Miranda-Martínez AY, González-Mora S, Bantim RAM, Lima
746 FJ, Pardo JD (2022) Digging deeper into colonial palaeontological practices in modern
747 day Mexico and Brazil. R Soc Open Sci 9(3):210898

748 Corecco L, Pereira VP, Soares MB, Schultz CL (2020) Geochemical study of the vertebrate
749 assemblage zones of the Santa Maria supersequence (middle to late triassic), Paraná
750 Basin, Brazil. Braz J Geol 50(4):e20200014

751 Corecco L, Bezerra FI, Silva Filho WF, Nascimento Júnior DR, da Silva JH, Felix JL (2022)
752 Petrological meaning of ethnostratigraphic units: laminated limestone of the Crato
753 Formation, Araripe Basin, NE Brazil. Pesq Geocienc 49(1):e121139

754 Custódio MA, Quaglio F, Warren LV, Simões MG, Fürsich FT, Perinotto JAJ, Assine ML
755 (2017) The transgressive-regressive cycle of the Romualdo Formation (Araripe Basin):
756 sedimentary archive of the Early Cretaceous marine ingression in the interior of
757 Northeast Brazil. Sediment Geol 359:1–15

758 Das N (1997) Chemostratigraphy of sedimentary sequences: a review of the state of the art.
759 JGSI 49(6):621–628

760 Donnely LJ, Pirrie D (2024) Crimes associated with geological materials: mining, minerals,
761 metals and fossils. Geol Today 40(4):159-164

762 Du F, Yang J, Zhao X, He X, Zhang P, Zhang J, Wang H, Kang Y (2025) Characteristics and
763 paleoenvironmental indications of caddisfly larval cases-stromatolite bioherms in the
764 Lower Cretaceous in Liupanshan Basin, Central China. Cretac Res 165:105973

765 Fačevicová K, Bábek O, Hron K, Kumpan T (2016) Element chemostratigraphy of the
766 Devonian/Carboniferous boundary – a compositional approach. Appl Geochem 75:211–
767 221

768 Fambrini GL, Silvestre DC, Barreto Junior AM, Silva-Filho WF (2020) Estratigrafia da Bacia
769 do Araripe: estado da arte, revisão crítica e resultados novos. Geol USP, Sér Cient
770 20(4):169-212

771 Fathy D, Wagreich M, Ntaflos T, Sami M (2021) Paleoclimatic variability in the southern
772 Tethys, Egypt: insights from the mineralogy and geochemistry of Upper Cretaceous
773 lacustrine organic-rich deposits. Cretac Res 126:104880

774 Figueiredo RG, Moreira JKR, Saraiva AÁF, Kellner AWA (2011) Description of a new
775 specimen of *Susisuchus anatoceps* (Crocodylomorpha: Mesoeucrocodylia) from the

776 Crato Formation (Santana Group) with comments on Neosuchia. Zool J Linn Soc
777 163(Supl):273–288

778 Garcia RJL, Silva Júnior JB, Abreu IM, Soares SAR, Araujo RGO, Souza ES, Ribeiro HJS,
779 Hadlich GM, Queiroz FS (2020) Application of PCA and HCA in geochemical
780 parameters to distinguish depositional paleoenvironments from source rocks. J S Am
781 Earth Sci 103:102734

782 Gelsthorpe D (2024) Repatriation and Decolonization of Geology Collections in an
783 Evolving Sector. Geoconserv Res 7(2)

784 Grawunder A, Merten D (2011) Rare earth elements in acidic systems – biotic and abiotic
785 impacts. In: Kothe E, Varma A (eds) Bio-geo interactions in metal-contaminated soils.
786 Springer, Berlin, Heidelberg, pp 81–97

787 Guo Q, Shields GA, Liu C, Strauss H, Zhu M, Pi D, Goldberg T, Yang X (2007) Trace element
788 chemostratigraphy of two Ediacaran–Cambrian successions in South China: implications
789 for organosedimentary metal enrichment and silicification in the early Cambrian.
790 Palaeogeogr Palaeoclimatol Palaeoecol 254(1-2):194–216

791 Hamid I, Lacerda LD, Saraiva AÁF, Sial AN, Benigno APA, Aguiar JE (2024a) Aptian–Albian
792 paleoenvironmental geochemistry: Araripe Basin, Northeastern Brazil. J S Am Earth Sci
793 137:104856

794 Hamid I, Martins MS, Saraiva AÁF, Benigno APA, Lima FJ, Bantim RAM, Sial AN, Aguiar
795 JE, Duong MTN, Dang DH, Lacerda LD (2024b) Geochemical analysis of mass
796 mortality events in the Cretaceous (Aptian) Konservatt-Lagerstätte of Crato paleolake,
797 Brazil. Palaeogeogr Palaeoclimatol Palaeoecol 655:112558

798 Hammer Ø, Harper DAT, Ryan PD (2001) PAST: Paleontological Statistics software package
799 for education and data analysis. Palaeontol Electron 4(1):1

800 Heimhofer U, Martill DM (2007) Stratigraphy of the Crato Formation. In: Martill DM, Bechly
801 G, Loveridge RF (eds) The Crato fossil beds of Brazil: window into an ancient world.
802 Cambridge University Press, UK, pp 25–43

803 Heimhofer U, Ariztegui D, Lenniger M, Hesselbo SP, Martill DM, Rios-Netto AM (2010)
804 Deciphering the depositional environment of the laminated Crato fossil beds (Early
805 Cretaceous, Araripe Basin, Northeastern Brazil). Sedimentology 57(2):677–694

806 Hinkle DE, Wiersma W, Jurs SG (2003) Applied statistics for the behavioral sciences.
807 Houghton Mifflin, Boston

808 Hubbard CR, Snyder RL (1988) RIR-measurement and use in quantitative XRD. Powder Diffr
809 3(2):74–77

810 Kellner AWA (2023a) Fósseis, leis e bom senso. Mesa redonda: Descolonização da
811 Paleontologia Brasileira (SBPC). Anais da 74ª Reunião Anual da SBPC (2022),
812 Sociedade Brasileira para o Progresso da Ciência, São Paulo, pp 1–5

813 Kellner AWA (2023b) Cultural objects at risk - the responsibility of reviewers and editors. An
814 Acad Bras Cienc 95:e2023951

815 Kellner AWA, Campos DA (2007) Short note on the ingroup relationships of the Tapejaridae
816 (Pterosauria, Pterodactyloidea). B Mus Nac - Geologia 75:1–14

817 Kellner AWA, Saraiva AÁF (2019) Fósseis da Chapada do Araripe - uma odisseia no Cretáceo/
818 Fossils from the Chapada do Araripe - A Cretaceous Odyssey. Pró-Imagem Produções
819 Fotográficas, 160 p

820 Kellner AWA, Maisey JG, Campos DA (1994) Fossil down feather from the Lower Cretaceous
821 of Brazil. Palaeontology 37(3):489–492

822 Kellner AWA, Campos DA, Sayão JM, Saraiva AÁF, Rodrigues T, Oliveira G, Cruz LA, Costa
823 FR, Silva HP, Ferreira JS (2013) The largest flying reptile from Gondwana: a new
824 specimen of *Tropeognathus* cf. *T. mesembrinus* Wellnhofer, 1987 (Pterodactyloidea,
825 Anhangueridae) and other large pterosaurs from the Romualdo Formation, Lower
826 Cretaceous, Brazil. An Acad Bras Cienc 85(1):113–135

827 Kowal-Linka M, Jochum KP, Surmik D (2014) LA-ICP-MS analysis of rare earth elements in
828 marine reptile bones from the Middle Triassic bonebed (Upper Silesia, S Poland): Impact
829 of long-lasting diagenesis, and factors controlling the uptake. Chem Geol 363:213–228

830 Kuhn CES, Carvalho IS, Reis FAGV, Spisila AL, Nolasco MC, Hach AH (2023) Ubirajara:
831 The dilemma of the Brazilian fossil curator. Geol Curat 11(7):469–479

832 Kuhn CES, Carvalho IS, Reis FAGV, Spisila AL, Nolasco MC, Hach AH, Strieder AJ (2024)
833 Brazilian fossils are not necessarily cultural heritage. Nat Ecol Evol 8(6):1050–1051

834 Lenharo M, Rodrigues M (2022) Movement to Decolonize Fossil Science Gains Steam. Nature
835 605:18-19

836 Lúcio T, Moura WAL, Albuquerque GCS, Souza Neto JA (2022) Tracing marine conditions
837 in the Ipubi Black Shales, Araripe Basin, NE Brazil: An approach by chemical elements
838 contents. J S Am Earth Sci 116:103880

839 Macário MA, Ghilardi AM, Santana EMG, Santos ES, Dal Molin A, Haertel LM, Aureliano
840 T, Pinheiro AP, Lima D, Salú ATO, Cisneros JC, Saraiva AÁF (2025) The study of fossil

macroinvertebrates from the Santana Group, Brazil: Legal and ethical challenges and neocolonial legacies in paleontology. Palaeontol Electron 28(3):1–48

Martill DM (2007) The age of the Cretaceous Santana Formation fossil Konservat Lagerstätte of north-east Brazil: a historical review and an appraisal on the biochronostratigraphic utility of its paleobiota. Cretac Res 28:895–920

Merli M, Bonadiman C, Pavese A (2020) Aluminium distribution in an Earth's non–primitive lower mantle. Geochim Cosmochim Acta 276:70–91

Michaelis Dictionary online (2026) Accessed in: 08/21/2026. Available in: <https://michaelis.uol.com.br/>

Montero-Serrano JC, Palarea-Albaladejo J, Martín-Fernández JA, Martínez-Santana M, Gutiérrez-Martín JV (2010) Sedimentary chemofacies characterization by means of multivariate analysis. Sediment Geol 228(3–4):218–228

Murtagh F, Contreras P (2012) Algorithms for hierarchical clustering: an overview. Wiley Interdiscip Rev Data Min Knowl Discov 2(1):86–97

Nagarajan R, Madhavaraju J, Nagendra R, Armstrong-Altrin JS, Moutte J (2007) Geochemistry of Neoproterozoic shales of the Rabanpalli Formation, Bhima Basin, northern Karnataka, southern India: implications for provenance and paleoredox condition. Rev Mex Cienc Geol 24(2):150–160

Nagendra R, Nagarajan R, Bakkiaraj D, Armstrong-Altrin JS (2011) Depositional and post-depositional setting of Maastrichtian limestone, Ariyalur Group, Cauvery Basin, South India: a geochemical appraisal. Carbonates Evaporites 26(2):127–147

862 Nascimento Júnior DR, Silva Filho WF, Erthal F (2024) Crato Lake Deposits: Rocks to
863 Preserve an Extraordinary Fossil Lagerstätte. In: Iannuzzi R, Rößler R, Kunzmann L
864 (eds) Brazilian Paleofloras: From Paleozoic to Holocene. Springer, Switzerland, pp
865 1017–1070

866 Neumann VHML (1999) Estratigrafía, sedimentología, geoquímica y diagénesis de los
867 sistemas lacustres Aptienses–Albienses de la Cuenca de Araripe (Noreste de Brasil).
868 Dissertation, Universidad de Barcelona

869 Neumann VH, Cabrera L (1999) Una nueva propuesta estratigráfica para la tectonosecuencia
870 post-rifte de la cuenca de Araripe, nordeste de Brasil. Boletim do 5° Simpósio sobre o
871 Cretáceo do Brasil, pp 279–285

872 Neumann VH, Borrego AG, Cabrera L, Dino R (2003) Organic matter composition and
873 distribution through the Aptian–Albian lacustrine sequences of the Araripe Basin,
874 northeastern Brazil. Int J Coal Geol 54(1–2):21–40

875 Nielsen F (2016) Hierarchical clustering. In: Nielsen F (ed) Introduction to HPC with MPI for
876 Data Science. Springer, pp 195–211

877 Oliveira GR, Kellner AWA (2017) Rare hatchling specimens of *Araripemys* Price, 1973
878 (Testudines, Pelomedusoides, Araripemydidae) from the Crato Formation, Araripe
879 Basin. J S Am Earth Sci 79:137–142

880 Paim PAV, Corecco L, Pereira VP, Soares MB (2025) Rare Earth Elements in Permo-Triassic
881 bones from the Paraná Basin, Brazil: a preliminary approach. Pesq Geocienc
882 52(2):e147543

883 Pimentel de Sousa MA, Nascimento Júnior DR, Bahniuk AM, Della Porta G (2025) Pilot Study
884 on Fingerprinting the Isotopic Signatures of Fossiliferous Limestones as a Tool for
885 Forensic Investigation of Fossil Trafficking (Cretaceous Crato Formation, Brazil).
886 Geosciences 15(10):403

887 Pinheiro FL, Horn BLD, Schultz CL, de Andrade JAFG, Sucerquia PA (2012) Fossilized
888 bacteria in a Cretaceous pterosaur headcrest. Lethaia 45(4):495–499

889 Ponte FC, Ponte Filho FC (1996) Estrutura geológica e evolução tectônica da Bacia do Araripe.
890 Departamento Nacional de Produção Mineral, Recife, 68 p

891 Pontes NV, Chagas DB, de Souza ACB, Nascimento Júnior DR, Silva Filho WF, Capilla R,
892 Garcia AJV, de Araújo Nogueira Neto J (2021) Organic and isotopic geochemistry of
893 evaporites and shales of the Santana Group (Araripe Basin, Brazil): clues on the evolution
894 of depositional systems and global correlation during the Lower Cretaceous. Minerals
895 11(8):795

896 Raja NB, Dunne EM, Matiwane A, Khan TM, Nätscher PS, Ghilardi AM, Chattopadhyay D
897 (2021) Colonial history and global economics distort our understanding of deep-time
898 biodiversity. Nat Ecol Evol 6(2):145–154

899 Ravidà DCG, Caracciolo L, Heins WA, Stollhofen H (2023) Towards an improved
900 discrimination and correlation of Permian–Lower Triassic sediments in Central Europe:
901 a chemostratigraphic approach. Sediment Geol 452:106408

902 Reimann C, de Caritat P (1998) Chemical elements in the environment: factsheets for the
903 geochemist and environmental scientist. Springer-Verlag, Berlin

904 Rodríguez-Cuicas ME, Montero-Serrano JC, Garbán G (2019) Paleoenvironmental changes
905 during the late Albian oceanic anoxic event 1d: an example from the Capacho Formation,
906 southwestern Venezuela. Palaeogeogr Palaeoclimatol Palaeoecol 521:10–29

907 Rosa MC, Morales N, Assine ML (2023) Transtensional tectonics during the Gondwana
908 breakup in northeastern Brazil: Early Cretaceous paleostress inversion in the Araripe
909 Basin. Tectonophysics 846:229666

910 Sacchi E, Nicosia U (2013) Forensic paleontology: A tool for “intelligence” and investigation.
911 J Forensic Sci 58(3):651-657

912 Salgado-Campos VMJ, Carvalho IS, Bertolino LC, Duarte TA, Araújo BC, Borghi L (2021)
913 Clay mineralogy and lithogeochemistry of lutites from the Lower Cretaceous Crato
914 Member, Araripe Basin, NE Brazil: implications for paleoenvironmental, paleoclimatic
915 and provenance reconstructions. J S Am Earth Sci 110:103329

916 Santos ES, Ribeiro SC, Feitosa AÁF, Kellner AWA, Simões TR (2025) A neotype and
917 reassessment of phylogenetic relationships of the fossil lizard *Calanguban alamoi* from
918 the Crato Formation (Early Cretaceous, Brazil). J Syst Palaeontol 23(1):2496536

919 Saraiva AÁF, Hessel MH, Guerra NC, Fara E (2007) Concreções calcárias da Formação
920 Santana, Bacia do Araripe: uma proposta de classificação. Estud Geol 17(1):40–57

921 Schober P, Boer C, Schwarte LA (2018) Correlation coefficients: appropriate use and
922 interpretation. Anesth Analg 126(5):1763–1768

923 Shannon RD (1976) Revised effective ionic radii and systematic studies of interatomic
924 distances in halides and chalcogenides. Acta Crystallogr A 32(5):751–767

925 Sial AN, Gaucher C, Ramkumar M, Ferreira VP (2018) Chemostratigraphy as a formal
926 stratigraphic method. In: Sial AN, Gaucher C, Ramkumar M, Ferreira VP (eds)
927 Chemostratigraphy Across Major Chronological Boundaries. Geophysical Monograph
928 Series, American Geophysical Union, pp 1–25

929 Stewens PP (2023) "*Ubirajara*" and *Irritator* Belong to Brazil: Achieving Fossil Returns
930 Under German Private Law. Int. J. Cult. Prop. 30(3):298-318

931 Storari AP, Rodrigues T, Bantim RAM, Lima FJ, Saraiva AÁF (2021) Mass mortality events
932 of autochthonous faunas in a Lower Cretaceous Gondwanan Lagerstätte. Sci Rep
933 11(1):6976

934 Suarez CA, Suarez MB, Terry Jr DO, Grandstaff DE (2007) Rare earth element geochemistry
935 and taphonomy of the Early Cretaceous Crystal Geyser Dinosaur Quarry, east-central
936 Utah. Palaios 22(5):500–512

937 Templ M, Filzmoser P, Reimann C (2008) Cluster analysis applied to regional geochemical
938 data: problems and possibilities. Appl Geochem 23(8):2198–2213

939 Toledo MCM., Pereira VP (2001) A variabilidade de composição da apatita associada a
940 carbonatitos. Rev Inst Geol 22(112):27–64

941 Turekian KK, Wedepohl KH (1961) Distribution of the elements in some major units of the
942 Earth's crust. Geol Soc Am Bull 72(2):175–192

943 Varejão FG, Silva VR, Assine ML, Warren LV, Matos SA, Rodrigues MG, Fürsich FT, Simões
944 MG (2021a) Marine or freshwater? Accessing the paleoenvironmental parameters of the
945 Caldas Bed, a key marker bed in the Crato Formation (Araripe Basin, NE Brazil). Braz J
946 Geol 51(1):e2020009

947 Varejão FG, Warren LV, Simões MG, Buatois LA, Mángano MG, Bahniuk Rumbelsperger
948 AM, Assine ML (2021b) Mixed siliciclastic–carbonate sedimentation in an evolving
949 epicontinental sea: Aptian record of marginal marine settings in the interior basins of
950 north-eastern Brazil. Sedimentology 68(5):2125–2164

951 Viana MS, Neumann VHL (2002) Membro Crato da Formação Santana, Chapada do Araripe,
952 CE - riquíssimo registro de fauna e flora do Cretáceo. In: Schobbenhaus C, Campos DA,
953 Queiroz ET, Winge M, Berbert-Born M (eds) Sítios geológicos e paleontológicos do
954 Brasil. CPRM/DNPM, Brasília, pp 113–120

955 Ward JH (1963) Hierarchical grouping to optimize an objective function. J Am Stat Assoc
956 58(301):236–244

957 Warren LV, Varejão FG, Quaglio F, Simões MG, Fürsich FT, Poire DG, Catto B, Assine ML
958 (2017) Stromatolites from the Aptian Crato Formation, a hypersaline lake system in the
959 Araripe Basin, northeastern Brazil. Facies 63(1):3–22

960 Wilby PR, Martill DM (1992) Fossil fish stomachs: a microenvironment for exceptional
961 preservation. Hist Biol 6(1):25–36

962 Wu T, Boak J, Birdwell JE (2022) Geochemical Studies of the Green River Formation in the
963 Piceance Basin, Colorado: II. Chemofacies from Hierarchical Cluster Analysis. Utah
964 Geological Association Publication

Supplementary Files

This is a list of supplementary files associated with this preprint. Click to download.

- TableS2HighandLows.xlsx
- TableS1SamplesID.doc
- TableS3Correlations.xlsx
- TableS4DEECPAASNormalizationEFCompleto.xlsx
- TableS5MineralPhaseIdentificationXRD.docx